

**REINFORCED SYNTACTIC FOAM SMC COMPOSITES FOR
AUTOMOTIVE LIGHTWEIGHTING**

A Dissertation
Presented to
The Academic Faculty

by

Arielle Elise Berman

In Partial Fulfillment
of the Requirements for the Degree
Master of Science in Mechanical Engineering in the
George W. Woodruff School of Mechanical Engineering

Georgia Institute of Technology
May 2020

COPYRIGHT © 2020 BY ARIELLE ELISE BERMAN

**REINFORCED SYNTACTIC FOAM SMC COMPOSITES FOR
AUTOMOTIVE LIGHTWEIGHTING**

Approved by:

Dr. Kyriaki Kalaitzidou, Advisor
G.W. Woodruff School of Mechanical Engineering
Georgia Institute of Technology

Dr. Jonathan S. Colton
G. W. Woodruff School of Mechanical Engineering
Georgia Institute of Technology

Dr. Robert J. Moon
The Forest Products Laboratory
USDA-Forest Service
School of Materials Science and Engineering
Georgia Institute of Technology

Date Approved: March 24, 2020

To my mom and dad, for their endless support

ACKNOWLEDGEMENTS

I would like to express my gratitude and appreciation for my research advisor, Professor Kyriaki Kalaitzidou. I would not be where I am today without her mentorship and support. Not only did she teach me how to conduct research, but she also demonstrated the invaluable skill of being an effective leader. I would like to thank Dr. Robert Moon for his advice throughout the past two years that greatly improved my research and technical writing. And, thank you to Professor Jonathan Colton, for being a member of thesis committee and taking the time to review and provide feedback on my master's thesis. Additionally, I would like to give my sincerest thanks to my colleague Eddie DiLoreto. I learned how to be a graduate student from observing him. We worked together to run the SMC, analyze the data, and create some of the figures in this thesis.

Thank you to my friends at Georgia Tech for their endless encouragement and for enriching my graduate school experience. I would not have been able to do this without the love and support from my boyfriend, Sean. Lastly, I want to thank my parents for loving me and believing me.

TABLE OF CONTENTS

ACKNOWLEDGEMENTS	iv
LIST OF TABLES	vii
LIST OF FIGURES	ix
LIST OF SYMBOLS AND ABBREVIATIONS	xii
SUMMARY	xiii
CHAPTER 1. Introduction	1
1.1 Sheet Molding Compounding (SMC)	1
1.2 Syntactic Foams	2
1.3 Water Uptake Studies	5
1.4 Research Motivation	8
1.5 Goals and Objectives	10
1.6 Organization of Thesis	12
CHAPTER 2. Materials and Methods	14
2.1 Materials	14
2.2 Processing Technique	17
2.2.1 Resin Paste Preparation	18
2.2.2 Sheet Molding Compound (SMC) Fabrication	20
2.2.3 Compression Molding	21
2.2.4 Determination of the GF content and density	22
2.2.5 Characterization Techniques	24
2.3 Composite Processing Characterization	25
2.3.1 Viscosity	25
2.3.2 Glass Fiber Content	28
2.3.3 Microstructure	30
2.4 Water Uptake Procedure	33
2.5 Chapter Summary	33
CHAPTER 3. Processing challenges	35
3.1 Incorporation of HGS	35
3.2 Glass Fiber Loading	35
3.3 Effect of Formulation on Manufacturability	38
3.4 SMC Handling	39
3.5 Minimization of Void Content	41
3.6 Chapter Summary	44
CHAPTER 4. Mechanical Properties Overview	45
4.1 Tensile Properties	45
4.2 Flexural Properties	47
4.3 Impact Properties	49

4.4	Ashby Plot	50
4.5	Chapter Summary	53
CHAPTER 5. Potential Reinforcing Mechanisms and Counteracting Phenomena		
	54	
5.1	Independent Variables and Corresponding Reinforcing Mechanisms	54
5.2	Chapter Summary	57
CHAPTER 6. JMP Statistical Analysis		58
6.1.1	All Formulations	58
6.2	Select Formulations	60
6.3	JMP Analysis of Mechanical Properties	63
6.3.1	Tensile Strength	64
6.3.2	Tensile Modulus	66
6.3.3	Flexural Strength	67
6.3.4	Flexural Modulus	69
6.3.5	Impact Properties	71
6.4	Chapter Summary	73
CHAPTER 7. Cost Analysis and Suggestions for Manufacturers		75
7.1	Formulation Cost Comparison	75
7.2	Suggestions for Manufacturers	78
7.3	Chapter Summary	78
CHAPTER 8. Water Uptake		79
8.1	Effect of Formulation on Water Uptake	79
8.1.1	Effect of Glass Surface Area on Water Uptake	80
8.1.2	Effect of CaCO ₃ on Water Uptake	83
8.2	Chapter Summary	85
CHAPTER 9. Conclusions and future work		86
9.1	Conclusions	86
9.2	Future Work	87
Appendix A. contour plots		89
A.1	Flexural Modulus Contour Plot	89
REFERENCES		90

LIST OF TABLES

Table 1	Advantages and disadvantages of SMC manufacturing [1].	1
Table 2	Typical properties of industry standard density SMC composites.	2
Table 3	Table of density, tensile strength, tensile modulus, and flexural strength found in literature for fiber reinforced syntactic foams. UPR was the matrix in all samples.	5
Table 4	Table of previous literature results for equilibrium water uptake (%) of UPR/GF SMC and bead-filled polyester composites. UPR was the matrix in all samples.	8
Table 5	List of the variables studied and their value ranges.	11
Table 6	HGS nomenclature, density, and dimensions.	15
Table 7	Resin paste formulation nomenclature, plate density, HGS vol%, and calculated GF vol%. Data are given as mean +/- one standard deviation.	17
Table 8	Table of resin paste compounding steps.	19
Table 9	Viscosity of formulations from Ares-M parallel plate rheometer.	26
Table 10	HGS loadings of low- and ultra-low density resin paste formulations for viscosity comparison.	26
Table 11	GF loading measurement techniques, weight percent values, and the target GF weight percent. Data is given as mean +/- one standard deviation .	29
Table 12	Table of residual cure time study during 7-day maturation period at room temperature. These results indicate that cure enthalpy plateaus after 3 days.	41
Table 13	IDI Composites International standard density tensile properties [37].	47
Table 14	IDI Composites International standard density tensile properties [37].	48
Table 15	Mechanical properties benchmarking from literature for Ashby Plot (Figure 20 & 21).	50

Table 16	Potential mechanisms of each composite variable that could affect the mechanical properties.	57
Table 17	Full-factorial DOE of all formulations that include HGS. Yellow highlight indicates which runs were completed in the present study.	59
Table 18	Mixed-level fractional factorial of all samples that include HGS [51].	60
Table 19	Input variables for JMP software for six formulations of interest.	61
Table 20	Full-factorial of six formulations shown in Table 19. Yellow highlight indicates which runs have been completed in this research.	62
Table 21	Fractional factorial DOE for formulations found in Table 19. This is an identical DOE to Taguchi Orthogonal Array for the same set of inputs.	63
Table 22	Summary of statistically significant variables affecting the mechanical properties of SMC fiber reinforced syntactic foam composites.	73
Table 23	Material-driven cost analysis of all formulations studied in this research.	77
Table 24	Values of solid surface free energy, liquid surface free energy, and contact angle used to calculate solid/liquid interfacial free energy and determine wettability [55–59].	83

LIST OF FIGURES

Figure 1	Component loadings, in volume percent, of typical SMC formulations [4].	3
Figure 2	Real-World Fuel Efficiency (miles per gallon) and CO ₂ emissions (grams/mile) through the years from the 2019 EPA Automotive Trends Report [26].	9
Figure 3	Figure showing GHG compliance performance (grams/mile) versus the EPA standard (grams/mile) [26].	9
Figure 4	Decreasing density values as HGS content increases and CaCO ₃ content declines.	12
Figure 5	Schematic of HGS showing outer radius, inner radius, and wall thickness. The outer diameter is double the outer radius, and the radius ratio is the inner radius divided by the outer radius.	15
Figure 6	Key steps of SMC UPR-GF-HGS composite processing.	17
Figure 7	(a) High shear Cowles blade (b) IKA Eurostar 20 mixer and (c) Schematic of “rolling donut” needed to achieve homogeneous mixing.	18
Figure 8	<i>Above:</i> Schematic of components of SMC line <i>Below:</i> Pilot-scale SMC at Georgia Tech.	21
Figure 9	Schematic of stacking of SMC plies by flipping alternating layers over the y-axis.	22
Figure 10	Viscosity behavior as a function of HGS vol% and type.	27
Figure 11	Viscosity of resin paste as a function of HGS density for spheres 32 (0.32 g/cm ³), 32-MS (0.32 g/cm ³), and 28 (0.28 g/cm ³).	28
Figure 12	SEM images of waterjetted surfaces: (a) L28: The fractured and resin-filled HGS indicate that the fracture occurred during processing when the matrix could still flow into the spheres, (b) U32: the HGS are fractured during sample cutting and not during manufacturing considering that they are empty, (c) L32: complete wetting of GF and HGS and infiltration of the resin into the roving.	32

Figure 13	Representative viscosity measurements comparing standard density (S) to low- (L32, L28) and ultra-low (U28, U32-MS) density formulation resin pastes.	37
Figure 14	Schematic of the ultra-low density formulation sticking to the doctor blade due to its high viscosity and elastic behavior.	39
Figure 15	GF pull out after only 5 days of room temperature maturation.	40
Figure 16	Results of pressure study showing density (g/cm^3) vs. pressure (MPa) and OM cross-sections. Porosity is no longer observed at P3 = 5.7 MPa.	43
Figure 17	Tensile strength and modulus of SMC formulations. Bars represent tensile strength, and circles represent tensile modulus.	46
Figure 18	Flexural strength and modulus of SMC composites. Bars represent flexural strength and circles represent flexural modulus.	48
Figure 19	Impact energy of SMC composites.	49
Figure 20	Ashby Plot of specific tensile properties comparing this study with results [11,32,35-38] on SMC composites and fiber reinforced syntactic foams. See Table 5 for definitions of A, B, C, D, and E.	52
Figure 21	Ashby Plot of specific flexural properties comparing this study with results [32,36,38] on SMC composites and fiber reinforced syntactic foams. See Table 5 for definitions of A, B, and E.	52
Figure 22	Schematic showing factor and level combinations used in a fractional factorial DOE.	62
Figure 23	JMP results for significant input variables that affect tensile strength.	64
Figure 24	JMP statistical comparison for tensile strength between the six formulations of interest.	65
Figure 25	Tensile strength (MPa) vs. HGS loading (vol%) of three sphere types.	65
Figure 26	JMP results for significant input variables that affect tensile modulus.	66
Figure 27	JMP statistical comparison for tensile modulus between six formulations of interest.	67

Figure 28	JMP results for significant input variables that affect flexural strength.	67
Figure 29	JMP statistical comparison for flexural strength between six formulations of interest.	68
Figure 30	Flexural strength (MPa) versus HGS loading (vol%) of three sphere types.	69
Figure 31	JMP results for significant input variables that affect flexural modulus.	69
Figure 32	JMP statistical comparison for flexural modulus between six formulations of interest.	70
Figure 33	Flexural modulus (GPa) versus HGS content (vol%) for spheres 28, 32, and 32-MS.	71
Figure 34	JMP results for significant input variables that affect impact energy.	71
Figure 35	JMP statistical comparison for impact energy between six formulations of interest.	72
Figure 36	Impact Energy (J/cm ²) versus HGS loading (vol%) for three HGS types.	72
Figure 37	Weight Gain (%) vs. Time (s ^(1/2)) of samples immersed in DIW at 70°C.	80
Figure 38	GF Total surface area of GF and HGS for S, M38, and L46 formulations.	82
Figure 39	Steady state weight gain (%) from water uptake.	82
Figure 40	Total calcium carbonate (CaCO ₃) surface area for S, Mδ, and Lα formulations.	84
Figure 41	JMP contour plot illustrating the effect of calcium carbonate content and HGS loading on the flexural modulus.	89

LIST OF SYMBOLS AND ABBREVIATIONS

HGS	Hollow Glass Sphere
UPR	Unsaturated Polyester Resin
SMC	Sheet Molding Compound
CaCO ₃	Calcium Carbonate
CAFE	Corporate Average Fuel Economy
GF	Glass Fiber
TBPB	tert-Butyl peroxybenzoate
S	Standard Density (1.9 g/cm ³)
M	Mid-Density (1.5 g/cm ³)
L	Low-Density (1.2 g/cm ³)
U	Ultra-Low Density (1.0 g/cm ³)
SEM	Scanning Electron Microscope
DSC	Differential Scanning Calorimetry
DOC	Degree of Cure
DIW	Deionized Water

SUMMARY

The fuel efficiency of vehicles can be increased by the lightweighting of autobody parts. To achieve this goal, this study focused on developing “syntactic foams”. Hollow glass spheres (HGS) were incorporated into unsaturated polyester resin (UPR), via a Sheet Molding Compound (SMC) line, in which the resulting product is a fiber reinforced syntactic foam. By replacing the heaviest filler, calcium carbonate (CaCO_3), of typical SMC resin paste with HGS, the density of SMC composites can be decreased from the industry standard of 1.9 g/cm^3 to 1.5, 1.2, and 1.0 g/cm^3 , called mid-, low-, and ultra-low density, respectively. The HGS characteristics investigated were density, diameter, loading level and surface functionalization. In all formulations investigated, the resin paste was kept at 40 vol%. The syntactic foam composites were characterized in terms of tensile, flexural, and impact properties and were compared to standard density ones. The viscosity and microstructure of every composite formulation were also analyzed. Statistical analysis of a design of experiments (DOE) of a limited set of runs was utilized, and it was concluded that there was no significant difference between the samples. Therefore, manufacturers should produce the most cost-effective formulations, in this case: S and L28.

The water uptake of samples with three different HGS loadings was also studied. The effect of HGS, GF, and CaCO_3 surface areas in the final composite were investigated and mechanisms for water absorption were discussed. It was shown that the low-density samples exhibited a 2.33 and an 8.53 percentage point increase in water uptake when compared to standard and mid-density, respectively.

CHAPTER 1. INTRODUCTION

1.1 Sheet Molding Compounding (SMC)

Sheet molding compounding (SMC) is a continuous process used to produce fiber reinforced thermoset composites. It can be produced with either short discontinuous or continuous fibers and is followed by compression molding for curing [1]. SMC technology was first introduced in the 1960s in Japan and Europe. The manufacturing technique was then brought to the United States in 1965 [1]. By the 1980s, SMC was pervasive. Now, it is the third most utilized polymer composite manufacturing process, after only injection molding and hand lay-up [1]. Table 1 shows the advantages and disadvantages of SMC and subsequent compression molding, which is of importance to understand the limitations of this composite manufacturing process.

Table 1: Advantages and disadvantages of SMC manufacturing [1].

Advantages	Disadvantages
<ul style="list-style-type: none">• Formulation Variability• Good Surface Finish• Minimal Material Scraps• Little Mold Preparation	<ul style="list-style-type: none">• Continuous Thickening of Resin• Variations in Rheological Properties• Emission of Styrene

SMC has a variety of applications including marine (watercraft and buoyancy systems), bathroom components (sinks and bathtubs), and automotive (interior body panels and fenders). Automotive applications were the focus of this research, and an SMC part is superior to a comparable steel part in many ways:

1. Achieves better, more complex geometries

2. Decreases weight by 20-35%
3. Higher strength-to-weight ratio
4. Better corrosion and damage resistance
5. 40% lower tooling cost

Epoxy, vinyl ester, and phenolic resins can all be used as polymer resins in an SMC. In this work, unsaturated polyester resin (UPR) was used due to its pervasiveness in the automotive industry [2,3]. Charles Fisk developed polyester as a matrix for glass-reinforced composites in the 1950s [1]. It was chosen for this study due to its low-cost, short cure time, and good mechanical properties [1]. Typical properties of industry standard SMC composites with CaCO₃ and 25 wt% GF, are shown in Table 2 [1].

Table 2: Typical properties of industry standard density SMC composites.

Property	Value
Density (g/cm ³)	1.85
Tensile Strength (MPa)	75
Tensile Modulus (GPa)	10
Flexural Strength (MPa)	170

The density of SMC composites used in industry has the potential to be reduced if HGS are used as a lightweight filler, creating what is called a “syntactic foam.”

1.2 Syntactic Foams

Fillers are a major component of composite formulations. As can be seen in Figure 1, they make up 33-43 vol% of SMC Class-A application formulations [4]. Typical fillers in polymer resin pastes are talc, mica, alumina, kaolin clays, and silica [1,4]. Inexpensive

fillers such as calcium carbonate, are used to add volume to the resin paste while minimizing the cost of the final product [1]. The choice of filler is determined by needs in manufactured composites including fire resistance and conductivity, modification of viscosity, or density reduction of the material [1].

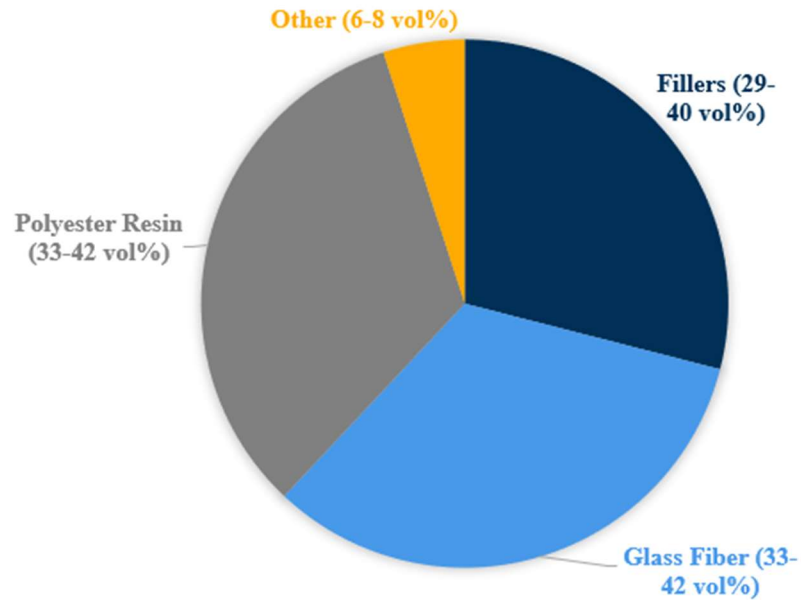


Figure 1: Component loadings, in volume percent, of typical SMC formulations [4].

To decrease composite density, hollow glass spheres can be incorporated into the resin paste to create what is referred to as a “syntactic foam.” Syntactic foams are a class of closed-cell foam, in which the gaseous phase is completely enclosed by the sphere [5]. Syntactic foam composites are stiffer, have higher modulus and strength, and create a more robust system when compared to open-cell foams, which have an interconnected pore structure [6,7]. This is because the glass walls of the HGS create micro-sandwich structures with the resin in between them [7]. When reinforcements are incorporated, such as discontinuous, chopped glass fiber (GF), then the system is then called fiber reinforced

syntactic foam, or “hybrid composite” [8,9]. Syntactic foams are of interest in marine applications, underwater pipe insulation, and aerospace sandwich structure core materials due to their low density and good compressive strengths [5,10].

Prior syntactic foams were also made from perlite spheres, phenolic spheres, and aluminum oxide ceramics [5]. They have been produced using fly ash cenospheres, a by-product of coal production. However, the inherent material flaws in these cenospheres make them inferior to HGS created specifically for this purpose [3,10]. SMC densities have been previously decreased from 1.9 g/cm³ to 1.2 g/cm³ [4]. The HGS dimensions, density, and surface treatment are the three HGS parameters of interest [3].

Hollow glass spheres do not behave as reinforcements in two- or three-phase syntactic foams. As a result, when creating composite formulations, it is necessary to maintain the glass fiber volume fraction to maintain properties to the greatest degree possible [4].

Table 3 lists existing research on fiber reinforced syntactic foams, produced with and without an SMC line [11,12]. It is seen that there are limited results for tensile strength, tensile modulus, and flexural strength with these composites systems. Most data is reported in the form of specific properties, which does not reveal the real effect of the HGS on the mechanical properties. Furthermore, the majority of current research into HGS/GF/UPR composites focuses on composites with low GF volume fraction. Besides Oldenbo, et al., who investigated HGS/GF/UPR SMC systems with 18-22 vol% GF, other studies reported on composites with densities below 1.0 g/cm³ but these were achieved with GF loadings less than 4.51 vol% [8,11–17]. While the composites studied by Oldenbo, et al. [11] have

comparable vol% GF to the composites of this study, their lowest reported density of around $\sim 1.57 \text{ g/cm}^3$ and the HGS used were not surface functionalized. Thus, there is a research gap in which the possibility of decreasing SMC composites to as low as 1.0 g/cm^3 with GF content between 10 and 16 vol% can be studied. Furthermore, as far as the author is aware, the effect of surface treated HGS on the properties of GF reinforced syntactic foams has not been investigated.

Table 3: Table of density, tensile strength, tensile modulus, and flexural strength found in literature for fiber reinforced syntactic foams. UPR was the matrix in all samples.

Sample Name	Reinforcement	Glass Spheres?	Density ³ (g/cm ³)	Tensile Strength (MPa)	Tensile Modulus (GPa)	Flexural Strength (MPa)	Citation
Std-SMC	GF	Yes	1.95	79	11.7	-	
Flex-SMC A	GF	Yes	1.57	69	8.6	-	[11]
Flex-SMC B	GF	Yes	1.58	79	8.3	-	
SF	N/A	Yes	0.67	-	-	37.4	
E1SF	GF	Yes	0.621	-	-	39.5	
E2SF	GF	Yes	0.633	-	-	39.1	
E3SF	GF	Yes	0.671	-	-	45.4	[12]
E4SF	GF	Yes	0.676	-	-	39.2	
E5SF	GF	Yes	0.72	-	-	49	

1.3 Water Uptake Studies

Previously, water uptake studies have been conducted on GF reinforced thermosets including epoxy, vinyl ester and polyester resin. However, experiments on syntactic foams, especially those that are reinforced, remain rare. Sauvante-Moynot, Gimenez, and Sautereau

studied the effect of water absorption on epoxy with untreated HGS [18], while Janas and McCullough compared neat unsaturated polyester resin (UPR) to a glass bead filled UPR system and a SMC composite system which was composed of polyester resin with glass fibers (GF) [19]. The absorption mechanisms of water into an immersed composite include (1) diffusion through the matrix and storage of the medium in the gaps between the polymer chains, (2) capillary flow of water along the fiber/matrix interface, particularly if voids exist between the two phases, and (3) storage of the immersion medium in microcracks [20–22]. Furthermore, there are two competing water absorption processes: *hydrolysis* and *hydrophilization*. Hydrolysis is the process in which, during submersion in a liquid medium, low molecular weight specimen, including styrene, are extracted from the polymer matrix [22–24]. It is notable that ester groups in the polymer matrix are particularly susceptible to hydrolysis [22]. Hydrophilization is the acceleration of water absorption and swelling. These two processes can be seen in a Weight Gain % vs. (time)^{1/2} figure, as hydrolysis accounts for the “shoulder” seen in the plot, as the weight of the sample is decreasing due to the leaching of water soluble molecules out of the composite. However, following this “shoulder,” the weight gain percent once again increases, creating a peak, prior to reaching steady-state due to the greater water uptake during hydrophilization [22]. During hydrophilization, plasticization of the resin matrix occurs. Plasticization is a result of the absorbed liquid causing the polymer chains to expand and increase the distance between each other. This causes hydrogen bonds to break, ultimately lowering the elastic modulus [20,24]. Glass is hydrophilic, as opposed to the hydrophobic nature of the resin matrix. Thus, it is expected that water absorption will rise as HGS volume is increased. Additionally, the addition of HGS increases surface area and creates

more interfaces within the composite. It is expected that there will be greater absorption in these cases because the water can percolate and be stored within these glass-matrix interfacial regions [20]. Water uptake is of importance because SMC is utilized as a structural material in bathtubs, boat hulls, autobody parts, and wave runners [1]. In the latter three applications, moisture absorption through either environmental humidity or direct submersion in water can alter the mechanical integrity of the composite parts.

Table 4 shows research published on the water uptake behavior of different SMC composites produced with GF [19,24,25]. Janas, et al. [19] found that the glass bead filled samples exhibited greater equilibrium water uptake compared to the neat UPR and SMC samples. As such, it is expected in this research that the inclusion of HGS in the composite will increase water absorption.

Table 4: Table of previous literature results for equilibrium water uptake (%) of UPR/GF SMC and bead-filled polyester composites. UPR was the matrix in all samples.

Sample Name	Reinforcement	Glass Spheres?	Temp (°C)	Equilibrium Water Uptake (%)	Citation
SMC-1	GF	No	70	3.9	
SMC-2	GF	No	70	4.2	
SMC-3	GF	No	70	3.5	[24]
SMC-4	GF	No	70	6.1	
SMC-5	GF	No	70	5.9	
SMC-25	GF	No	23	3.6	
SMC-65	GF	No	23	3.5	[25]
SMC-30 EA	GF	No	23	2.95	
Unfilled	N/A	No	60	2.1	
Bead Filled	N/A	Yes	60	5.93	[19]
SMC-R65	GF	No	60	3.22	

Water uptake of UPR/GF SMC as well as syntactic foams have been studied previously. However, the water uptake in hybrid systems of UPR/GF/HGS SMC composites, especially those containing surface treated HGS has not been investigated.

1.4 Research Motivation

The need for more fuel-efficient vehicles is driven by consumer demand as well as federal policies. It can be seen in Figure 2 that, as fuel efficiency increases, CO₂ emissions per mile decrease.

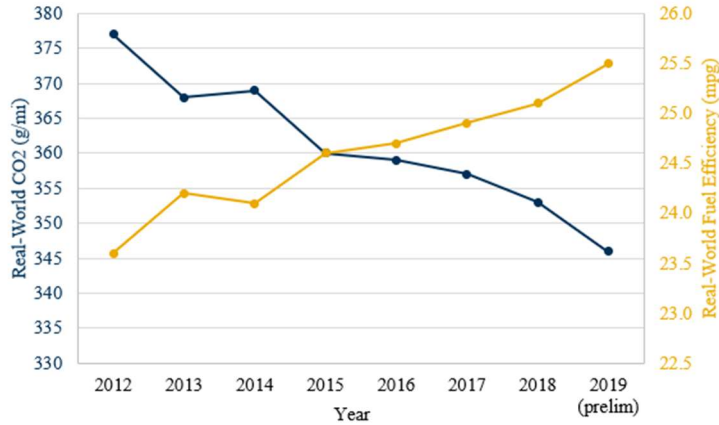


Figure 2: Real-World Fuel Efficiency (miles per gallon) and CO₂ emissions (grams/mile) through the years from the 2019 EPA Automotive Trends Report [26].

As a result, to comply with the continuously decreasing Environmental Protection Agency (EPA) Greenhouse Gas (GHG) emissions standards (Figure 3), automotive companies are looking for novel techniques to decrease the mass of their vehicles [26].

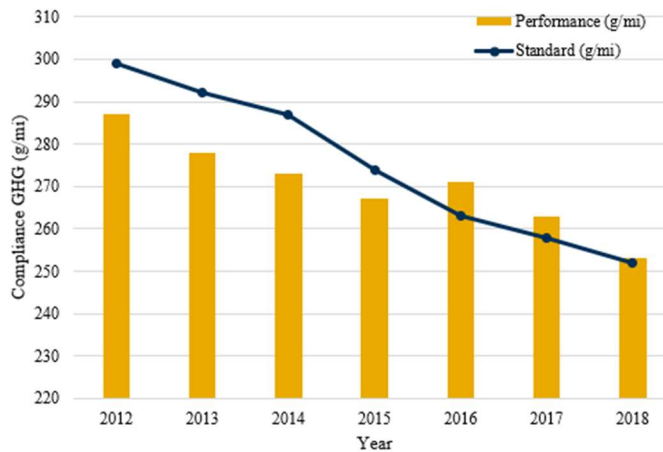


Figure 3: Figure showing GHG compliance performance (grams/mile) versus the EPA standard (grams/mile) [26].

A promising path forward is the creation of a new Sheet Molding Compounding (SMC) resin that utilizes hollow glass spheres (HGS), with densities ranging from 0.28 to

0.46 g/cm³, in place of high density fillers, in particular calcium carbonate (CaCO₃) which has a density of 2.71 g/cm³.

1.5 Goals and Objectives

The goal of this study is to develop lightweight SMC composites from unsaturated polyester resin formulations containing HGS. The idea is to use HGS as a replacement for the much heavier CaCO₃, which is commonly used in typical GF/UPR SMC composites as filler for cost reduction. The goal will be achieved by the following objectives and corresponding tasks:

Objective 1: Understand the effect of HGS characteristics on the ability to process the SMC composites.

Objective 2: Understand the effects of HGS characteristics on the mechanical properties, water uptake and density of the HGS/GF/UPR SMC composites.

The HGS properties that were studied include the following: density, dimensions, loading level, and surface functionalization (Table 5). As the composite density decreases, the CaCO₃ content decreases while HGS loading increase. Thus, mechanical properties are investigated as a function of CaCO₃ content as well.

Table 5: List of the variables studied and their value ranges.

Variables Studied	Value Range
HGS Density (g/cm^3)	0.28 – 0.46
HGS Diameter (μm)	20 – 44
HGS Wall Thickness (μm)	0.57 – 1.16
HGS Loading (vol%)	19 – 44
HGS Surface Functionalization	Untreated; Methacrylsilane
CaCO_3 Loading (vol%)	0 – 64.32

These aspects are all integral to furthering understanding of the mechanical properties of lightweight SMC composites. This exploratory study seeks to lower SMC composite densities from the industry standard density of 1.9 g/cm^3 to 1.5 g/cm^3 , 1.2 g/cm^3 , and even as low as 1.0 g/cm^3 (Figure 4), while maintaining mechanical properties.

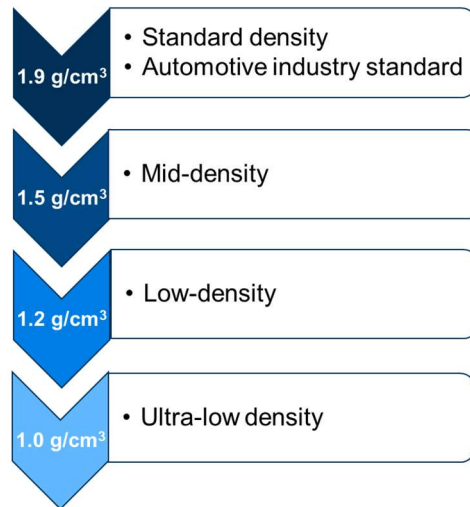


Figure 4: Decreasing density values as HGS content increases and CaCO₃ content declines.

It is hypothesized that GF loading (vol%) and HGS loading (vol%) will be the two factors with the most significant influence on the mechanical properties. Additionally, it is predicted that HGS surface functionalization will have a greater effect on the properties in ultra-low density, in which the HGS loading is higher.

1.6 Organization of Thesis

This thesis consists of nine chapters:

Chapter (1): Introduction to SMC composites, syntactic foams, and water uptake mechanisms are presented. This chapter also includes the goals, objectives, and motivation.

Chapter (2): Materials and methodologies of compounding as well as shaping are discussed.

Chapter (3): This chapter presents processing challenges of manufacturing various lightweight SMC formulations.

Chapter (4): An overview of the tensile, flexural, and impact properties of syntactic foams is provided. These results are compared to those of the standard density SMC composite and typical industry values.

Chapter (5): Independent variables and resulting potential mechanisms that could affect mechanical properties are discussed.

Chapter (6): This chapter examines design of experiment (DOE) arrays and JMP statistical analysis.

Chapter (7): A cost analysis is completed, and suggestions for future manufacturers is provided.

Chapter (8): Water uptake behavior as well as the effect of glass surface and calcium carbonate surface area are considered.

Chapter (9): Conclusions and suggestions for future work are presented.

CHAPTER 2. MATERIALS AND METHODS

2.1 Materials

A two-part Unsaturated Polyester Resin (UPR) system of a 1:1 vinyl ester:unsaturated ester blend (Arotran 774) and a low profile additive polymer blend (Arotran 775) was supplied by Ashland, Inc. This resin system was specifically designed for lightweight systems and has a density of 1.07 and 1.05 g/cm³ for the two resin components, respectively. The calcium carbonate (CaCO₃) filler used, Hubercarb W4, was supplied by Huber Engineered Materials. BYK Additives provided the wetting agent, BYK 9010. The initiator, tert-Butyl peroxybenzoate (TBPB) was purchased from Sigma-Aldrich, the magnesium oxide thickener, AM9033, was obtained from Chromaflow Technologies and the Zinc Stearate, used as mold release agent, was produced by Acros Organics. The GF rovings, Advantex P204, were provided courtesy of Owens Corning. Five types of HGS were provided by 3M, four of which were not surface functionalized: iM16K, S32HS, S28HS, and S38HS, while one was functionalized with a methacrylsilane (3-(Trimethoxysilyl)propyl methacrylate): S32HS-MAS-1 (see Table 6). These HGS have differing diameters and wall thicknesses (Figure 5) resulting in true HGS densities between 0.28 and 0.46 g/cm³.

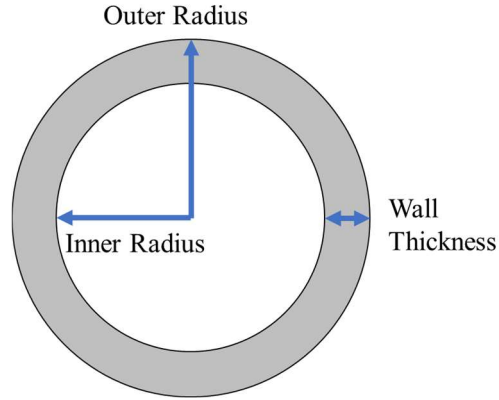


Figure 5: Schematic of HGS showing outer radius, inner radius, and wall thickness. The outer diameter is double the outer radius, and the radius ratio is the inner radius divided by the outer radius.

The radius ratio (η) and the wall thickness (t) were calculated using Eq. (1) and Eq. (2), respectively, and their values can be found in Table 6. ρ_{mb} is the HGS true density, while the particle material density, ρ_g , is glass density (2.54 g/cm^3) in this case. Furthermore, R_i and R_o are the inner and outer radii, respectively.

$$\eta = \left(1 - \frac{\rho_{mb}}{\rho_g}\right)^{1/3} = \frac{R_i}{R_o} \quad \text{Eq. (1)}$$

$$t = R_o(1 - \eta) \quad \text{Eq. (2)}$$

Table 6: HGS nomenclature, density, and dimensions.

HGS Type	HGS Name	Density (g/cm^3)	Outer Diameter (μm)	Radius Ratio (η)	Wall Thickness (μm)
S28HS	28	0.28	30	0.96	0.57
S32HS	32	0.32	25	0.96	0.58
S38HS	38	0.38	44	0.95	1.16
iM16k	46	0.46	20	0.94	0.64
S32HS-MAS	32-MS	0.32	25	0.96	0.58

Various HGS types had to be utilized because only spheres of certain densities could be used to achieve low- and ultra-low density composites. Resin paste formulations, seen in Table 7, were compounded with various combinations of glass sphere type and loading. The letters “S,” “M,” “L,” and “U” are used to represent SMC composites with standard density 1.94 g/cm³; mid-density of 1.5 g/cm³; low-density of 1.2 g/cm³; and ultra-low density of 1.0 g/cm³, respectively. In each case, the target resin content in the composite formulation was kept at 40 vol% for adequate wetting of the HGS and GF rovings.

The formulation dictates the amount of HGS needed to reach a target density. With increasing HGS loading, the GF weight fraction increases while the target GF volume fraction remains in the 15-20 vol% range. This is possible because, as the matrix density decreases, the GF weight fraction must increase to keep the GF volume fraction constant. The intended design principle for the SMC formulations was to maintain the GF content at approximately 15-20 vol%. The GF vol% was held constant to provide a more direct comparison between samples. By maintaining the GF vol% any effect of the GF on the mechanical properties would be normalized in the data. However, the experimentally determined true GF content proved that this target vol% was not always achieved. Thus, the differences in the actual GF loading may contribute to discrepancies in mechanical properties between formulations and mask any effect the HGS may have on the composite properties.

The S38HS is an industry standard, while the M38 formulation is of particular industrial relevance as it was a HGS with which manufacturers are already comfortable. For low- and ultra-low density composites, the novel HGS types (e.g., iM16K, S32HS, S28HS) were utilized.

Table 7: Resin paste formulation nomenclature, plate density, HGS vol%, and calculated GF vol%. Data are given as mean +/- one standard deviation.

Sample Name	Resin Paste Density (g/cm ³)	Composite Density (g/cm ³)	HGS vol%	GF vol%
S	1.75	1.94±0.002	-	22
M38	1.23	1.51±0.012	19	20
L28	0.86	1.08±0.010	33	13
L32	0.86	1.07±0.012	35	12
L46	0.83	1.11±0.006	38	16
L32-MS	0.86	1.12±0.017	34	15
U28	0.69	0.94±0.003	43	13
U32	0.70	0.89±0.009	44	10
U32-MS	0.70	0.98±0.013	42	15

2.2 Processing Technique

The processing steps to produce and test the SMC specimens can be seen in Figure 6.

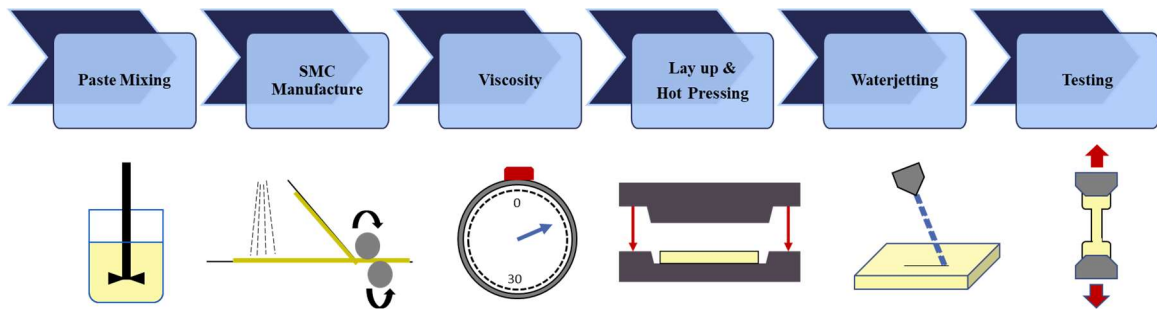


Figure 6: Key steps of SMC UPR-GF-HGS composite processing.

2.2.1 Resin Paste Preparation

The resin paste was compounded using a Cowles blade (Figure 7a) attached to an IKA Eurostar 20 mixer (Figure 7b). A 4 liter container with approximately 2.4 L of final material was used so that the mixing blade was positioned equally from the sides and bottom of the container (~3.8 cm) to create “rolling donuts” for quality dispersion of the materials (Figure 7c) [27].

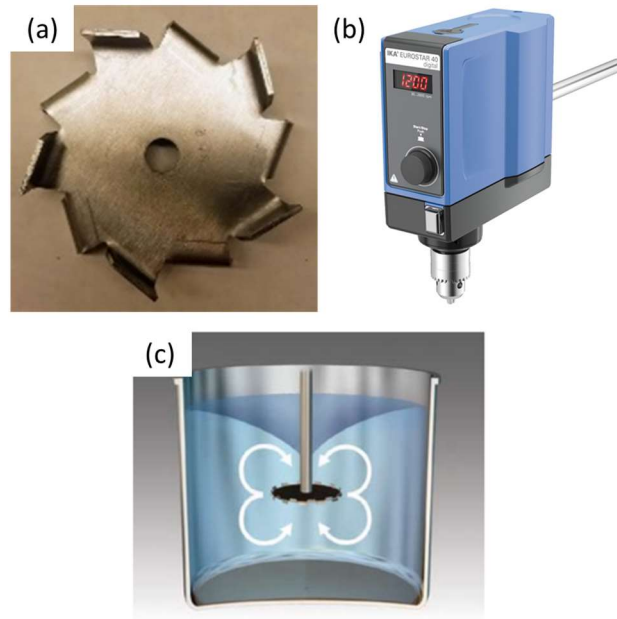


Figure 7: (a) High shear Cowles blade (b) IKA Eurostar 20 mixer and (c) Schematic of “rolling donut” needed to achieve homogeneous mixing.

The resin paste compounding process can be seen in Table 8. First, Arotran 774, Arotran 775, TBPB, and BYK 9010 were combined. Then, CaCO_3 and zinc stearate were gradually added at a speed of 2000 rpm. This mixing velocity was held for 3 mins. Next, for the mid-, low-, and ultra-low density formulations, the HGS were slowly incorporated at 1200 rpm to prevent their breakage. The mixer was kept at 1200 rpm until the resin paste

reached 35°C or for 10 mins. Finally, AM9033 was added and mixed for 3 mins at either 2000 rpm for standard density or 1200 rpm for all other formulations. The order in which the components were added was of importance because it affected the viscosity and thus the manufacturability of the formulation. For example, the solids, CaCO₃ and zinc stearate, were added first because they require mixing at higher velocities to break up agglomerates and make the paste homogeneous. Once the solids were fully incorporated, the HGS were added at a lower rpm to prevent fracture of the spheres. Finally, the time-based thickener, magnesium oxide, was added. This was necessary because, if it was added any earlier in the process, the viscosity would increase and prevent sufficient mixing of the other components into the resin paste.

Table 8: Table of resin paste compounding steps.

Compounding Step	Component
<i>A-side</i>	
#1	Liquid Resins (Arotran 774 and Arotran 775)
#2	Solids (CaCO ₃ , Zinc Stearate)
#3	Mixing at 2000 rpm for 3 minutes
#4	HGS
#5	Mixing at 1200 rpm for 10 minutes (or to 35°C)
<i>B-side</i>	
#6	Thickener (Magnesium Oxide)
#7	Mixing at 1200 rpm for 3 minutes

2.2.2 Sheet Molding Compound (SMC) Fabrication

Upon completion of the compounding, the resin paste was split equally between the upper and lower reservoirs of the SMC line, built by Finn & Fram, Inc. (Figure 8). One carrier film moved underneath each of the reservoirs carrying the resin paste under doctor blades at a set height. This deposited a resin layer of the desired thickness on each carrier film. A cutting roller chops the GF rovings into 2.54 cm fibers and continuously dropped them onto the lower carrier film in a random orientation over a 25.4 cm width. The lower and upper carrier films met and go through a compression zone, which ensures better wetting of the GF rovings and other solids within the resin, and the resulting material collected at the end of the line was in form of a 30 cm wide sheet. These uncured SMC sheets, approximately 2.5 m long, were folded and stored in a nylon bag and wrapped in aluminum foil to prevent the volatilization of styrene, which decreases the degree of crosslinking in the final composite. The SMC sheets were kept at room temperature to mature for 7 days to improve handling and increase viscosity to required levels for hot-pressing.

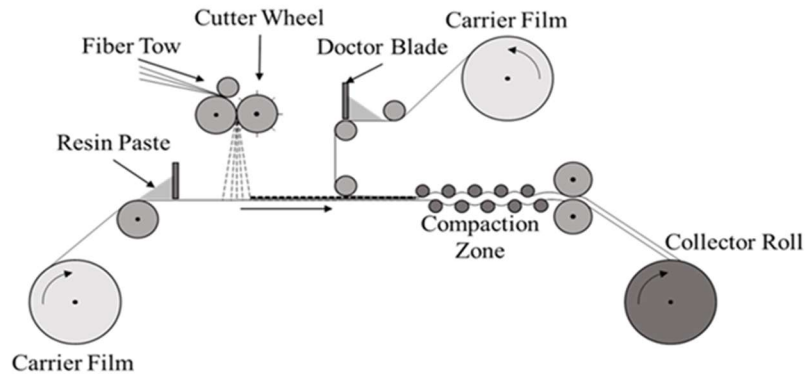


Figure 8: Above: Schematic of components of SMC line Below: Pilot-scale SMC at Georgia Tech.

2.2.3 Compression Molding

For SMC composite processing, square plies with edge lengths approximately 20.5 cm were cut from the uncured SMC sheet. The carrier film was then removed, and three or four plies were stacked while flipping each alternating layer over the y-axis to minimize the effect of any off-axis bias along the SMC direction (Figure 9).

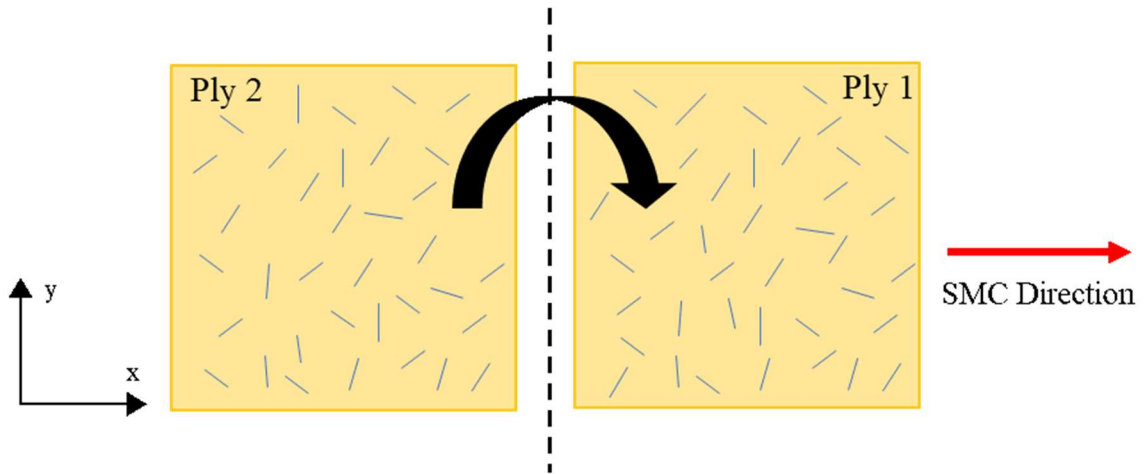


Figure 9: Schematic of stacking of SMC plies by flipping alternating layers over the y-axis.

Zinc stearate powder was applied to the 28 cm x 28 cm aluminum mold and heated until it melted. Allowing the zinc stearate to liquify gave the composite the best surface finish. Then the stack of plies, or charge, was placed in the preheated mold and cured in a Wabash 50 ton hot press, model v50-1818-2tmx, under approximately 44.7 metric tons of force (5.7 MPa of pressure) at 146°C for 2 mins. The final composite plate was removed from the mold and cut into mechanical testing coupons with their long axis along the SMC direction with a waterjet and then stored at room temperature.

2.2.4 Determination of the GF content and density

One cannot rely on the settings of the SMC line to determine the amount of GF in the SMC sheet and thus the resulting density of the final SMC composite. This is due to the inherent randomness in the SMC line and a lack of certainty in the amount of GF that are contained within the SMC width during production. Also, the density of the uncured

SMC is different than that of the final SMC composite due to entrapped air in the GF rovings that is expelled when the fibers are completely wetted by resin flow during the compression molding process.

The GF content was determined for the uncured SMC material by two methods: acetone dissolution (ASTM D3529-16) and burn-off (ASTM D2584-18), which is a method commonly used for thermoset composites [28][29][30]. Both techniques use a 2.54 cm diameter circle punchout that was removed from the uncured SMC material within 10 mins after processing. Acetone dissolution of the as-made SMC was used to determine the GF content and calibrate the SMC line to meet the targeted GF content. This is the most relevant and attractive method to industry because it leads to quick adjustment of the production parameters. Burn-off of uncured SMC cutouts was used as a comparison to the acetone dissolution method. This is necessary because the latter has the risk of losing small pieces of GF, which are cut off at the edge of the punch out and could pass through the sieve, resulting in an erroneously low GF content. During acetone dissolution, the sample was weighed without the carrier film, and then it was submerged in and rinsed with acetone at 320 Hz for 2 mins and 160 Hz for 2 mins on an IKA AS130.1 shaker table. It was filtered through a sieve in between. The remaining GF was manually washed with acetone until the acetone runs clear. The mass of the GF compared to the original mass of the sample gives the approximate wt% GF of the uncured SMC sheet. For the burn-off method, the punchout sample was placed in a Fisher Scientific IsoTemp Muffle Furnace from 300°C to 550°C increasing the temperature 100°C every hour until 500°C, and after an additional hour the temperature was increased to 550°C and left overnight. The final mass of the

remaining solids was used to calculate the GF loading in the SMC composite. These samples were approximately 5 grams.

The density of the SMC composite plates was estimated by water displacement using a density determination kit according to ASTM D792-13 and it was also calculated using the average measured dimensions, and mass of the entire plate. The density values were averaged over three samples for every formulation.

2.2.5 Characterization Techniques

A Leica DVM 6 Optical Microscope was used to study the microstructure including dispersion and distribution of GF and HGS, the presence of voids and wetting of GF. For higher resolution imaging, a Phenom ProX desktop scanning electron microscope (SEM) at an acceleration of 15 kV was used. SEM samples were sputter coated with gold to reduce charging during imaging.

A TA Differential Scanning Calorimetry Q2000 (DSC) was used to determine the degree of cure (DOC) and how it changes during the SMC maturation stage as well as the DOC of the final composites. Three samples of ~5 mg were tested in TA Instruments Tzero aluminum pans for each formulation. Samples were heated from 30°C to 300°C at 10°C/min.

The tensile, flexural and impact properties of the composites were determined as a function of the HGS characteristics. ASTM D638 standard Type I was followed to obtain tensile properties on an Instron 5982 with a 100 kN load cell. The preload for each test was 440 N/min up to 40N. Flexural data were acquired according to ASTM D790-17 on an

Instron 33R 4466 with a 500N load cell. The sample dimensions were 117 mm x 20 mm with 5-6 mm thickness and the testing was performed at room temperature with a three-point bending fixture with a span length of 85 mm at a test rate of 4.54 mm/min. Impact properties were determined according to ASTM D4812-11 with an Charpy Instron Pendulum Impact Tester. Impact specimens of 5-6 mm thickness are cut with dimensions of 63.5 mm x 12.7 mm and tested with a 30 kg anvil at a latch angle of 136° at room temperature. A minimum of four coupons were tested for every composite formulation

The viscosity of the A-side resin paste (described in Table 8) was acquired using an Ares-M Rheometer with 25 mm parallel plates. The resin was held in a 1 mm gap and tested at 0.5 s⁻¹. Data was collected for 3 mins following 5 mins of pre-shear.

2.3 Composite Processing Characterization

2.3.1 Viscosity

The viscosity of the resin paste at different stages in the SMC production is perhaps the most important material parameter for good process control. It determines the ease of mixing during compounding of the resin paste, the manufacturability of the SMC, the GF content of the SMC sheet, and the handling of the plies during lay-up. The HGS type and amount changes the viscosity of the resin paste prior to the addition of the thickener (Table 9). Within each target density set, samples containing S28HS had the lowest viscosity. M38 maintained the mechanical properties to the greatest extent probably due to the relatively lower viscosity and thus better wetting of the GF.

Table 9: Viscosity of formulations from Ares-M parallel plate rheometer.

Resin Paste Sample Name	Viscosity (Pa.s)
S	124
M38	110
L28	101
L32	151
L46	120
L32-MS	179
U28	185
U32	239
U32-MS	342

This study then focuses on resin paste produced with spheres 28, 32, and 32-MS. This is due to these HGS types having comparable sphere loadings at both low- and ultra-low formulations (Table 10).

Table 10: HGS loadings of low- and ultra-low density resin paste formulations for viscosity comparison.

HGS Type	Name	HGS Loading (vol%)
S28HS	L28	33
	U28	43
S32HS	L32	35
	U32	44
S32HS- MAS	L32-MS	34
	U32-MS	42

In Figure 10, one can see that the viscosity increases with HGS loading for all sphere types, due to the increased friction from the higher probability of HGS coming into contact with each other [31] and of course because solids are added in the resin. Another study showed that viscosity increases most with microsphere loadings above 40 vol%, with which ultra-low density formulations coincide [32]. Additionally, as anticipated, the surface functionalized HGS, have drastically higher viscosities than their un-surface modified counter parts. The stronger interactions between the modified HGS and the resin makes the material more resistant to shear [31].

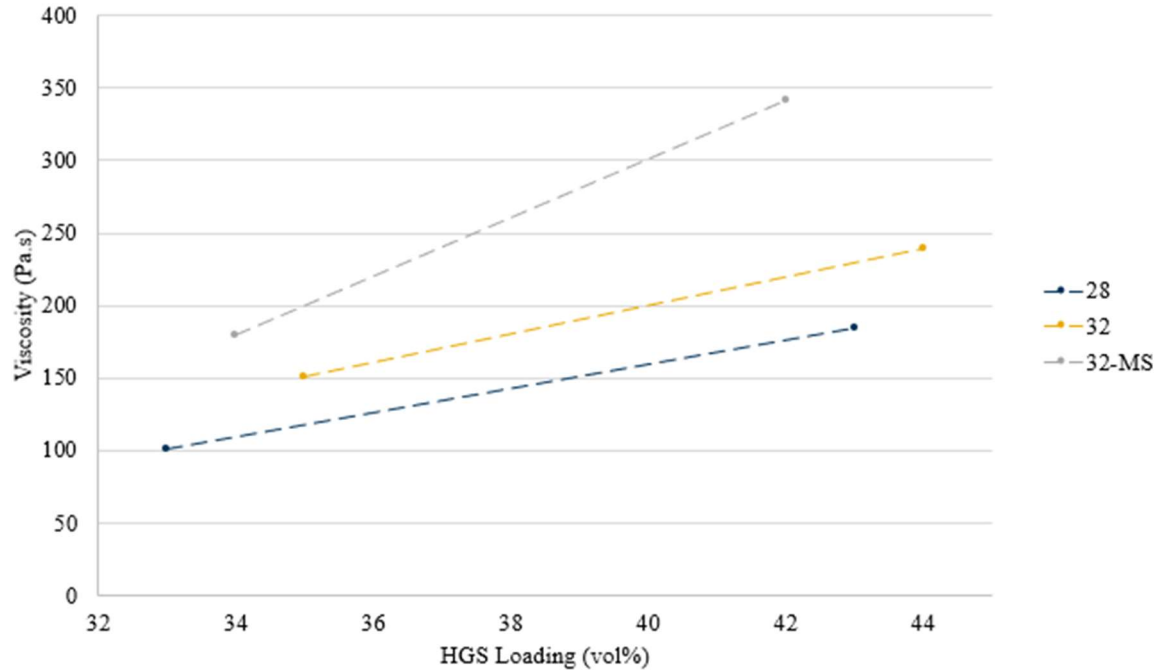


Figure 10: Viscosity behavior as a function of HGS vol% and type.

The viscosity also decreases as HGS density decreases, meaning that sphere 28 creates a resin paste with a lower mixing viscosity than either sphere 32 or 32-MS (Figure 11). This is probably due to higher density spheres being more resistant to flow. Resin flow within fiber bundles will be discussed in Section 2.3.3.

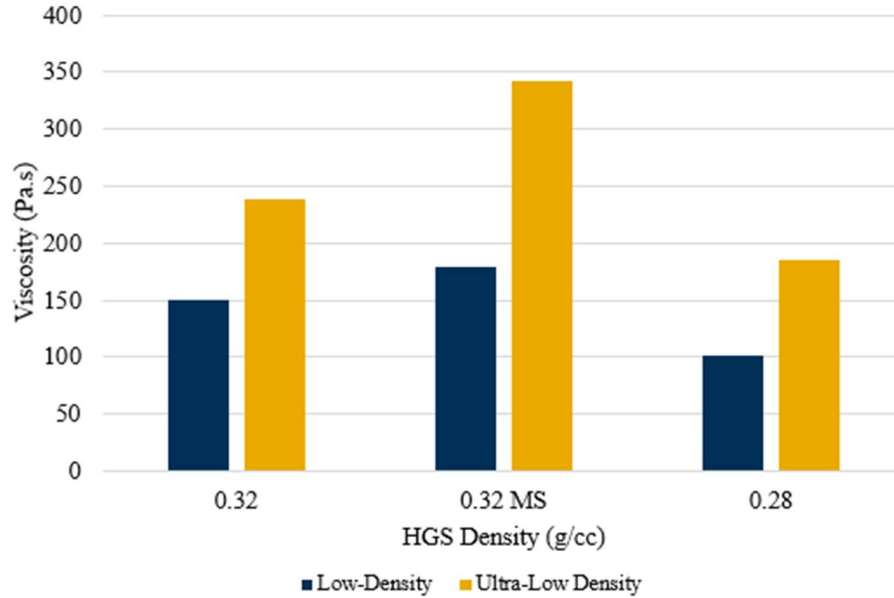


Figure 11: Viscosity of resin paste as a function of HGS density for spheres 32 (0.32 g/cm³), 32-MS (0.32 g/cm³), and 28 (0.28 g/cm³).

2.3.2 Glass Fiber Content

Three techniques for estimating the GF loading were used to compare actual GF weight percent to the target value and, subsequently, to adjust the SMC parameters to more closely approach the target GF loading. Three samples for each formulation were used to account for local variation. Following hot-pressing, the GF loading was calculated using the Rule of Mixtures and density from water displacement. While it is expected that the acetone dissolution technique will be an underestimate due to short pieces of fiber cut during the preparing of the sample falling through the sieve, Table 11 appears to suggest that acetone dissolution shows a higher GF loading than burn-off of the uncured SMC. This could be due to insufficient washing of the SMC material, leaving residual CaCO₃ or resin paste. This residue would cause the final mass to be larger than the actual weight of the GF, which would adversely affect the weight percent calculation. With all formulations, it

is expected that there will be a moderate standard deviation as well as variation across different GF content measurement techniques and when compared to the ideal target GF loading. This is due to the error of the measurement technique itself and to the randomness of the SMC material. Since the samples are being produced in a “real” pilot system, the weight percent of components will not be as exact or as consistent as on a benchtop scale. In addition, there is the inherent randomness in the SMC process, particularly with the distribution of cut GF on the carrier film, so ideal conditions cannot be achieved. Therefore, there will be differences in GF loadings between samples.

Table 11: GF loading measurement techniques, weight percent values, and the target GF weight percent. Data is given as mean +/- one standard deviation .

Sample	GF wt% (Acetone)	GF wt% (Burnoff)	GF wt% (From Density)	Target GF wt%
S	25.9 ± 2.2	24.6 ± 0.7	29.5 ± 0.5	29
M38	36.9 ± 2.9	32.7 ± 3.6	35.0 ± 2.5	36
L28	32.3 ± 2.4	34.2 ± 1.4	30.3 ± 2.6	42
L32	34.8 ± 4.8	34.2 ± 1.0	29.2 ± 2.8	42
L46	40.0 ± 1.5	36.4 ± 5.0	36.6 ± 1.6	42
L32-MAS	33.7 ± 0.4	28.0 ± 4.2	34.6 ± 4.0	42
U28	42.2 ± 1.5	43.6 ± 1.9	Not Available	42.4
U32	37.8 ± 2.0	34.2 ± 2.0	Not Available	40.5
U32-MAS	37.2 ± 3.0	36.5 ± 3.9	Not Available	40.5

2.3.3 *Microstructure*

Based on DSC residual enthalpy results, all plates have an unsaturated polyester resin percent cure of >97%. SEM imaging of the composite cross-sections (e.g., waterjet cut surfaces) was used to assess the integrity of the HGS and the degree of wetting of the resin with HGS and GF in the final composite. It is important to assess if HGS were damaged during the manufacturing process, and if so, when it occurred. If the fractured HGS were still hollow, it signifies they were broken during the cutting of the testing coupons. In contrast, if the fractured HGS were filled with resin, the fracture event occurred during mixing or compression molding and the resin was able to flow into the cracked HGS and cure. This has a negative consequence of increasing the density of the composite and should be avoided.

Resin filled HGS were uncommon in composite cross-sections for all HGS types, indicating that the processing conditions (e.g., 1200 rpm during mixing and the pressure during compression molding) inflicted minimal damage on the HGS. An example of a resin filled HGS is shown in Figure 12a, where the circular fractured outline of the L28 HGS wall can be seen; and on either side of the wall is the rough surface texture of the resin. This indicates that HGS were filled with resin before curing. This was the exception however, because in the case of U32 and L32, seen in Figures 12b and 12c, nearly all the HGS appear to be either intact and remain hollow or crushed having a smooth glassy surface texture indicating that the resin was fully cured prior to waterjetting the final composite. Empty, fractured HGS, mainly seen in Figure 12b, can contribute to lowering the density of the composites. This shows that HGS in the mid-, low-, and ultra-low density

plates were not broken during hot-pressing at 5.7 MPa which was higher than the 3.4 MPa recommended by Ashland. Inc.

Lastly, all composites had complete wetting of the resin to both the GF and HGS, as shown in representative images in Figure 12. This confirms that the resin paste viscosity was low enough to infiltrate the GF rovings and that there was a sufficient amount of resin in the formulation for complete filling (e.g., no dry spots). Mechanical properties are improved when the individual GF strands in the roving have good contact with the resin, as seen in Figure 12c, as dry spots prevent load transfer from the matrix to the reinforcement. HGS can also be seen between the fibers in the GF roving, further proving that resin flow was sufficient.

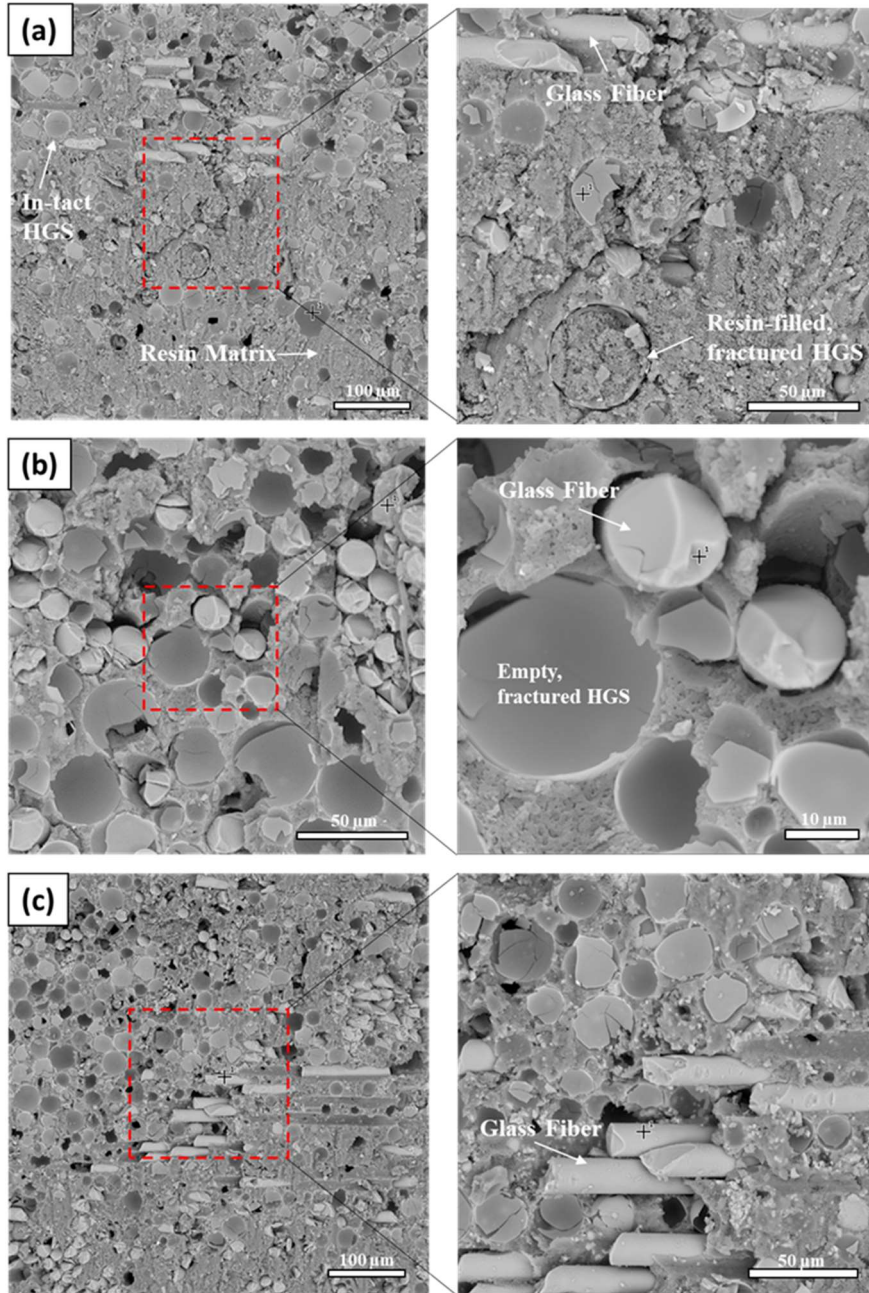


Figure 12: SEM images of waterjetted surfaces: (a) L28: The fractured and resin-filled HGS indicate that the fracture occurred during processing when the matrix could still flow into the spheres, (b) U32: the HGS are fractured during sample cutting and not during manufacturing considering that they are empty, (c) L32: complete wetting of GF and HGS and infiltration of the resin into the roving.

2.4 Water Uptake Procedure

Water uptake experiments based on ASTM D5229 were conducted by immersing 1.27 cm x 1.27 cm square composite coupons and measuring the mass increase periodically. Specifically, the coupons were dried for 24 hrs at 100°C then submerged in deionized water (DIW). Although that standard states that each square should weigh more than 5 grams, all samples in this study were between 1.4-2.6 grams due to limited availability of composite material. Samples were immersed at both 70°C and 35°C, to replicate the temperature at which these composites would be used on a hot day. Samples were removed from the immersion bath every three days, patted dry with Kimwipes, weighed, and quickly returned to the DIW. Weight gain percent was calculated using Eq. (3)

$$\frac{W_w - W_o}{W_o} \times 100\% \quad \text{Eq. (3)}$$

where W_w is sample mass after immersion for a particular period of time and W_o is dry mass of sample prior to immersion. Water uptake square coupons were said to have reached equilibrium water absorption when the percent change between two consecutive weighings was less than 0.02%, which took approximately 42 days.

2.5 Chapter Summary

In this chapter, the materials used to create reinforced syntactic foams were introduced. These included the resin matrix, the five HGS types and their properties, and the GF rovings. The steps of SMC composite manufacturing – paste mixing, SMC processing, and compression molding – were then detailed. Furthermore, the characterization steps of

viscosity, acetone dissolution, resin burn-off, and SEM microstructure analysis, and procedures for mechanical testing and water uptake were discussed.

In the next chapter, the major processing challenges overcome during production of low- and ultra-low density composites will be examined.

CHAPTER 3. PROCESSING CHALLENGES

Every change in resin paste formulation creates different challenges during compounding, SMC production, and compression molding. Understanding the ways in which these obstacles can be overcome is important to enable production at scale. This chapter will discuss five challenges that were overcome on the pilot scale, and what approach industry may take to ensure the manufacturability of ultra-low formulations.

3.1 Incorporation of HGS

Due to the extremely low density of the HGS, the process of mixing them into the thick resin paste can be difficult, particularly in the 1.0 g/cm^3 formulations. The ultra-low density resin behaves in such a way that achieving a “rolling donut” with the Cowles blade is difficult, so the HGS have a tendency to sit on top of the resin. As a result, it was necessary after 3 minutes of mixing at 1200 rpm to fold the HGS into the resin paste manually with a flat spatula to achieve adequate wetting of the filler. Very high HGS loading may compromise production rate due to need for increased mixing, however this was only at the benchtop scale. A mixer with higher maximum torque or a customized mixing blade may be able to remedy this issue in industrial settings.

3.2 Glass Fiber Loading

Glass fiber loading is dependent upon multiple SMC process and material parameters with the most dominant one being the viscosity of the resin. When the resin paste is pulled under the doctor blade by the carrier film, the viscosity will determine whether the observed thickness of deposited polymer on the carrier film is the same as the

doctor blade set height. Figure 13 compares representative viscosity data for standard, low-, and ultra-low density formulations. It is evident that all formulations show varying degrees of shear thinning behavior. While the rheological behavior of U28 and U32-MS is similar to that of S, there are greater differences in the low-density formulation results. At low shear rates, L32 has lower viscosity than S while L28 has higher viscosity than S. This behavior may have affected the amount of resin deposited onto the carrier film by the doctor blade. Depending on the belt speed (i.e. shear rate), each formulation may behave in a manner differently than that of the standard density formulation. As a result, if the viscosity is lower than expected, the resin may spread out after being deposited on the carrier film. This could lead to higher GF content. Consequently, the belt speed may need to be changed in an attempt to get closer to the target GF vol%, but this may once again affect the viscosity of the resin paste system.

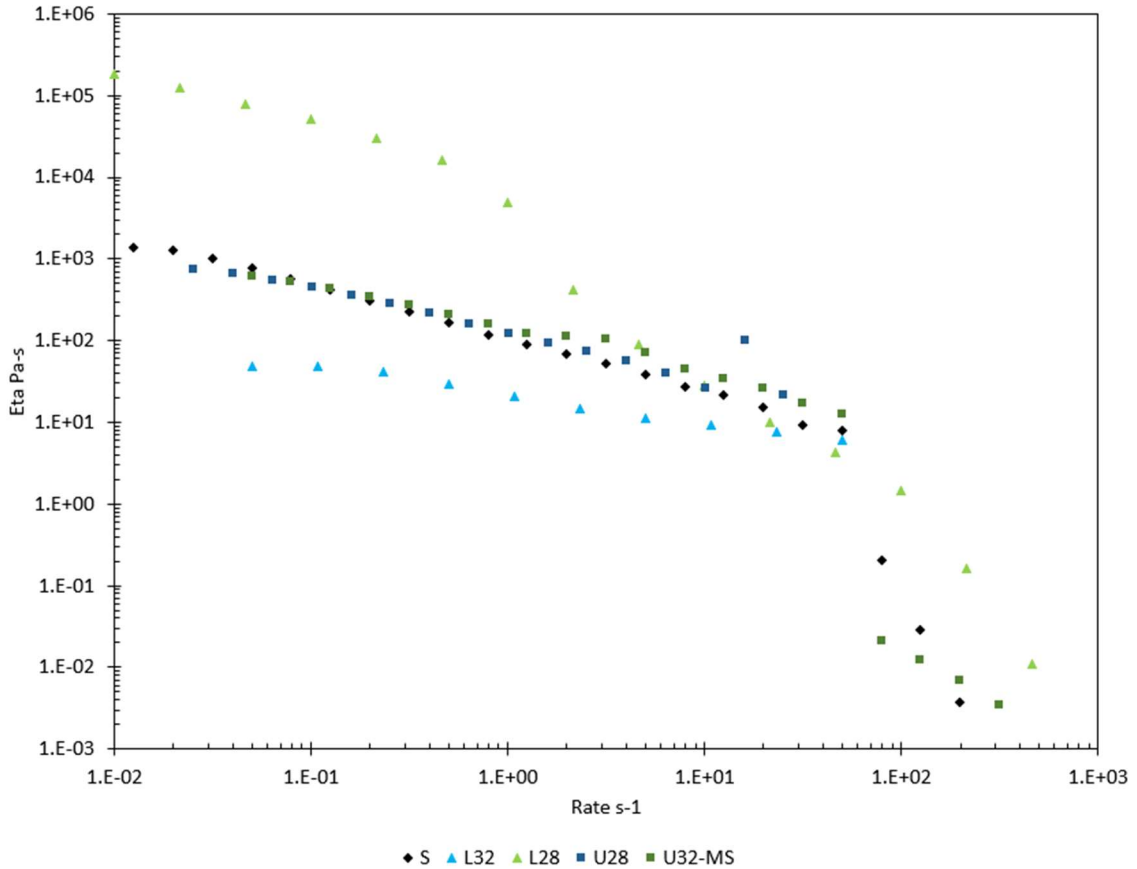


Figure 13: Representative viscosity measurements comparing standard density (S) to low- (L32, L28) and ultra-low (U28, U32-MS) density formulation resin pastes.

The two manufacturing pathways that were determined to have the most success of consistently increasing GF content was to increase the CaCO₃ volume percent during compounding and to decrease the SMC belt speed. Because the volume percent of GF in every formulation was designed to be 20 vol%, it was initially decided that the doctor blade height at 1.7 mm and a belt speed of 18.24 mm/s would be kept constant for every formulation. However, after GF loading confirmation, for any formulations in which these parameters did not achieve the target GF wt%, one of the two possible processing changes were made. If the viscosity was low and there was significant squeeze-out in the

compaction zone, the viscosity would need to be increased. This was possible in cases where the resin content was more than 40 vol%, which is necessary for proper wetting of the fillers and GF. In cases with lower resin content, the belt speed was decreased to increase GF vol%.

The reason for increasing the calcium carbonate volume percent from 1.52 vol% to 4.50 vol% was to increase the viscosity of some formulations so that they would behave in a more consistent manner when pulled under the doctor blade. This method also enabled an increase in GF content without altering the SMC parameters, which would require calibration, trial and error, and multiple run attempts to be determined. On the other hand, the decrease of the belt speed was to increase the glass fiber loading per unit length of the SMC material. While this did require multiple attempts to reach the correct fiber loading, it was more effective than changing the doctor blade height as it is unknown how that will change the flow of the resin going underneath it.

3.3 Effect of Formulation on Manufacturability

The resin paste formulation type also affected the ease of manufacturability when using the SMC line. After depositing the resin paste into the SMC line reservoirs, it was observed that while the standard, mid-, and low-density formulations flowed under the doctor blade without issue, the ultra-low density did not. It appeared that since it was so light, it tended to stick to the doctor blade (Figure 14) and had to be manually scraped onto the carrier film in order to be carried under the doctor blade. While this solution worked on an experimental scale, it would not be reasonable for large-scale industry production.

Future manufacturers could utilize viscosity modifiers to lower the viscosity of ultra-low density composite formulations.

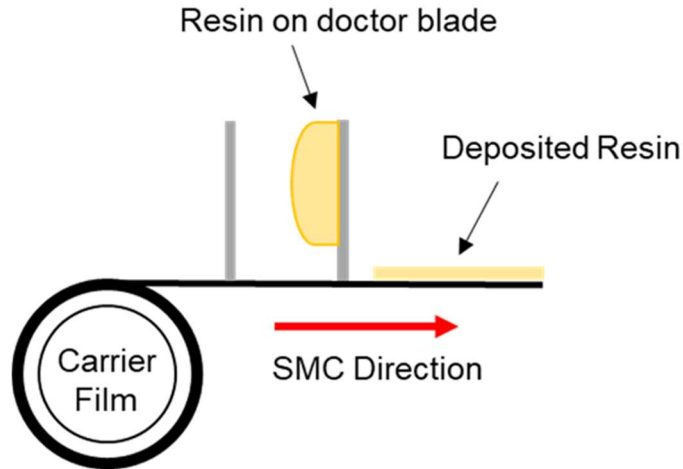


Figure 14: Schematic of the ultra-low density formulation sticking to the doctor blade due to its high viscosity and elastic behavior.

3.4 SMC Handling

Maturation of the SMC at room temperature is necessary to allow the material to thicken for easier handling, removal of the carrier film sheets, and successful compression molding. If the material has too low a viscosity, peeling off the carrier film removes GF and resin along with it (Figure 15). However, if it is at room temperature for too long, the SMC acts similarly to a solid and does not flow during compression molding. Ashland, Inc. recommends a maturation time of 5-7 days (Personal Contact: Thomas Skelskey), so a study was conducted to compare handling, compression molding, and composite properties after a 5-day versus a 7-day resin maturation time. There appeared to be no obvious differences in flow during compression molding, and it was also found that there was no significant difference in tensile properties between these two time periods.



Figure 15: GF pull out after only 5 days of room temperature maturation.

Additionally, the cure enthalpy of the samples was tested once a day from the time of SMC compounding (Day 0) to the day of compression molding (Day 7). Three samples across the width of the uncured SMC—one from the center and one from each lateral edge—were tested each day of the maturation period. The results showed that cure enthalpy plateaued after 3 days (Table 12). The cure kinetics of the final hot-pressed plate were equivalent on Day 5 and Day 7. As a result, only the ease of handling is affected by the SMC set-up time. While waiting 7 days prior to hot-pressing slowed down production rate of plates, it was needed to prevent the pull out of fibers during carrier film removal, which if extreme, may negatively affect mechanical properties of the final part.

Table 12: Table of residual cure time study during 7-day maturation period at room temperature. These results indicate that cure enthalpy plateaus after 3 days.

Day	Enthalpy (J/g)		
	<i>Center</i>	<i>Edge 1</i>	<i>Edge 2</i>
0	72.8	112.2	108.4
1	69.3	58.6	48.2
2	50.2	47.2	57.5
3	53.2	45.7	48.3
4	41.4	45.0	58.2
7	41.2	29.7	42.8

3.5 Minimization of Void Content

Considering that voids act as stress concentrations and can lead to premature failure of the composite, the void content must be minimized. This is most commonly accomplished by increasing the pressure during compression molding as pressure helps remove trapped gasses between and within SMC plies and pushes out volatiles byproducts of the curing reaction. The pressure recommended by Ashland, Inc. for the standard density composite plates was 7.2 MPa and for the mid- and low-density plates was 3.4 MPa (Personal Contact: Thomas Skelskey). In this study a pressure of 5.7 MPa was used, which was the maximum possible pressure as dictated by the capacity of the hot press and mold tool employed. A pressure study was conducted using an 18 cm x 18 cm mold to

understand/quantify the effect of pressure on the mechanical properties and understand the limitations imposed by using the hot-press.

The pressures used in this study were $P_1=1$ MPa, chosen as a baseline, $P_3 = 5.7$ MPa, which was the max pressure that the 45.4 metric tons hot press can apply on the 28 cm x 28 cm mold used to produce the test plates and $P_2=2.8$ MPa and $P_4=8.4$ MPa which are pressure values equally spaced around the pressure of interest. It is shown in Figure 16 that when almost no pressure was applied, i.e., $P_1=1$ MPa, extremely large voids can be seen in the cross-section optical images. In the same figure, slightly smaller, but still prominent, voids are present when the pressure was $P_2=2.8$ MPa. At $P_3=5.7$ MPa, no voids can be seen in the cross-section indicating higher expected mechanical properties. There appears to be no difference in noticeable void content between $P_3=5.7$ MPa and $P_4=8.4$ MPa, which indicates that a greater pressure during compression molding was not necessary. Though 8.4 MPa was not achievable using the Wabash hot-press on a 28cm x 28cm mold, this study shows that 5.7 MPa (P_3 in Figure 16) was sufficient to minimize void content in the composite.

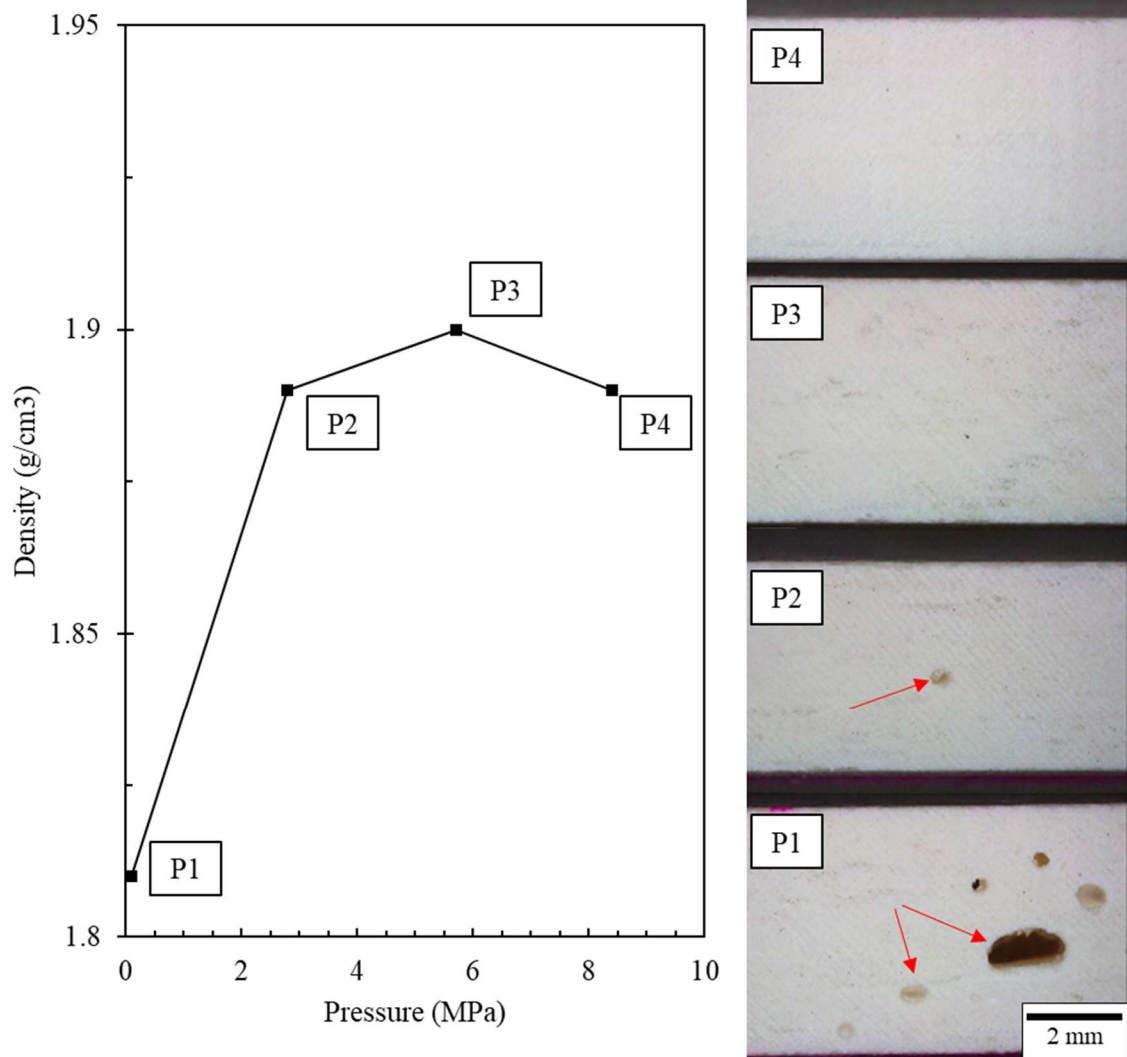


Figure 16: Results of pressure study showing density (g/cm^3) vs. pressure (MPa) and OM cross-sections. Porosity is no longer observed at P3 = 5.7 MPa.

As a result, a pressure of 5.7 MPa was used to produce all subsequent composites in this study. This was the maximum pressure possible given the hot-press limitations and the mold tool size. Such a pressure was higher than the 3.4 MPa recommended by the resin supplier for mid- low- and ultra-low density plates, but SEM showed no significant fracture of HGS at this higher pressure. Thus, the use of the greater pressure of 5.7 MPa on formulations with high HGS content, can minimize the void content without compromising

the lightweighting ability of the spheres. Both OM and SEM imaging are needed to find the optimal pressure to achieve the best mechanical properties without fracturing HGS, which would result in an increase of the density of the final composite.

In the case of standard density composites, a pressure of 7.2 MPa was recommended which was not possible using the available equipment configuration. Thus, it is noted that composites of standard density made in industry may have superior properties than the standard density composites made in this study due to the presence of micro voids caused by a relatively lower processing pressure.

3.6 Chapter Summary

This chapter discussed the processing challenges of producing lightweight SMC and the possible solutions to overcome them. The manufacturing obstacles that were solved during paste mixing included: incorporation of HGS into ultra-low density resin paste. SMC manufacturing challenges consisted of control of glass fiber loading and the effect of formulation on SMC processing, while minimization of void content was the main point of interest during hot-pressing.

In the next chapter, the tensile, flexural, and impact properties of lightweight SMC composites are analyzed.

CHAPTER 4. MECHANICAL PROPERTIES OVERVIEW

The previous chapter discussed the manufacturing challenges. Once these were resolved to the best of the author's ability, the composite plates were produced, and testing coupons were cut via waterjet. These coupons were then subjected to mechanical testing. An overview of the results are presented in this chapter. GF vol% is provided for each sample in all tensile, flexural, and impact results plots.

4.1 Tensile Properties

Assessing the outcome of the HGS filler characteristics such as diameter, true density, surface functionalization, and quantity (vol%) on the mechanical properties is important for understanding which sphere type and content is ideal for specific applications. Composites with HGS and GF, were compared in terms of their mechanical properties to composites of the standard density formulation.

The tensile strength and modulus results are shown in Figure 17. Most notably, M38 and L46 were the only two formulations that somewhat maintain the properties of the standard density composite, although they were both slightly lower. L46 apparently has a higher tensile strength and modulus than other low-density composites. Still, comparing the effect of the independent variables (HGS density, HGS diameter, CaCO₃ content) be challenging, as there is variation in the GF content. Within this data set, only samples of equivalent or similar GF content (vol%) can be directly compared. For example, the results can be compared within the following sets: S and M38, L32-MS and U32-MS, L28 and U28, as well as L46 and L32-MS. Nevertheless, due to the large standard deviations and

multiple, simultaneously changing inputs, no significant conclusions can be made without statistical analysis. This will be explored in Section 6.3.1 and 6.3.2.

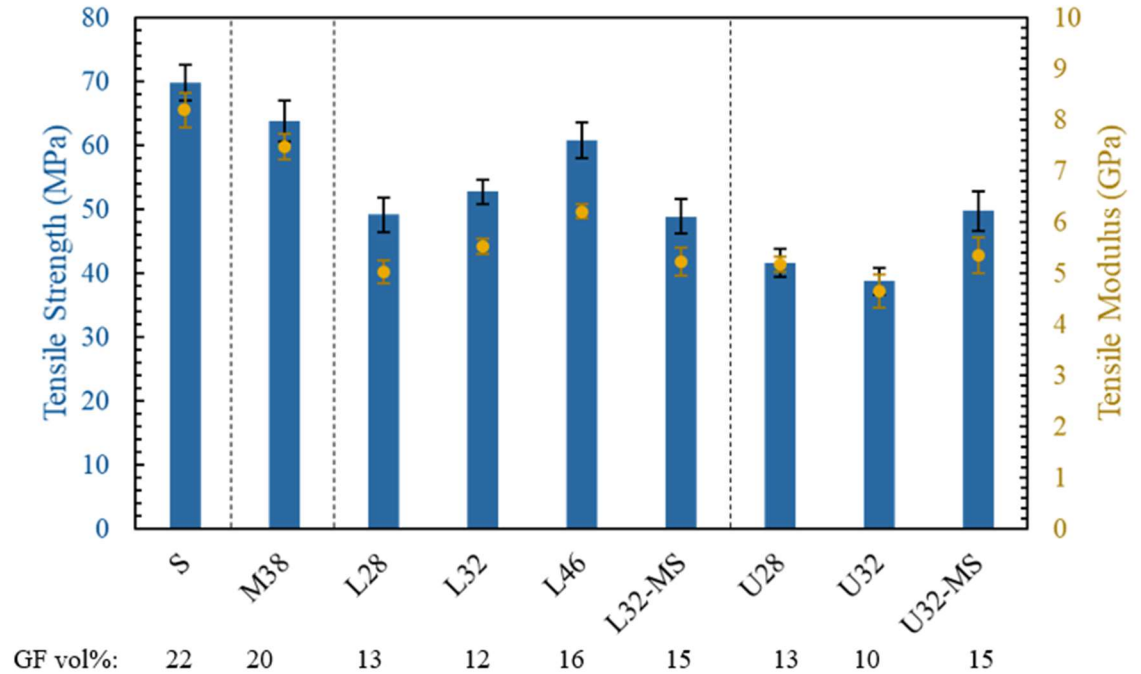


Figure 17: Tensile strength and modulus of SMC formulations. Bars represent tensile strength, and circles represent tensile modulus.

The tensile properties were compared to those of industry standard density SMC composites with 20 vol% GF (Table 13) [33]. As expected, the results detailed in Figure 17 are lower in some respects than those in industry, the latter of which can achieve higher pressure during hot-pressing. Only formulations S and M38 were able to meet the typical industry tensile strength. However, L46 is comparable considering that the GF content is only 16 vol% compared to the 22 or 20 vol% of standard (S) and mid-density (M38) composites; and allows for a reduction from 1.9 to 1.2 g/cm³. None of the samples produced achieved the industry tensile modulus.

Table 13: IDI Composites International standard density tensile properties [37].

IDI Composites International (GF 20 vol%)	
Tensile Strength (MPa)	62
Tensile Modulus (GPa)	15

4.2 Flexural Properties

Flexural strength and modulus results are shown in Figure 18. A surprising result was that the mid-density formulation has competitive flexural strength to that of the standard density. There is a general reduction in properties of the low- and ultra-low density compared the baseline standard density but this is also attributed to the lower GF vol%. Once again, only sample sets with equivalent GF vol% can be directly compared. These comparable groups are the same as those listed in Section 4.1. Statistical analysis to determine which formulations result in significantly different flexural strength and modulus will be discussed in Section 6.3.3 and 6.3.4, respectively.

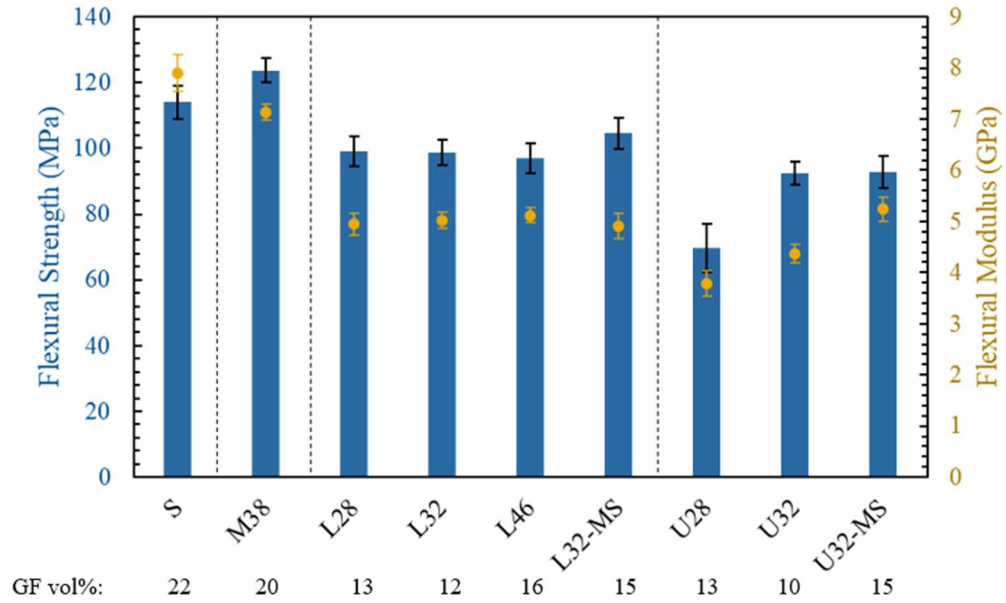


Figure 18: Flexural strength and modulus of SMC composites. Bars represent flexural strength and circles represent flexural modulus.

The flexural strength and modulus were compared to IDI Composites International standard density values (Table 14), both of which are much greater than the results achieved in this research. Once again, this could be due to the greater pressure that can be applied with larger hot-presses in industry, the resin and the GF type used.

Table 14: IDI Composites International standard density tensile properties [37].

IDI Composites International (GF 20 vol%)	
Flexural Strength (MPa)	158
Flexural Modulus (GPa)	14

4.3 Impact Properties

Impact energy is an indication of the ability of the composite to absorb energy at a high rate before fracture [34]. Interestingly, none of the samples fractured completely during Charpy testing but were held together by their high GF loading content. In the same way that tensile and flexural properties could only be compared between sets of samples with close to equal GF content, impact properties must also be analyzed in this way. Though, it is again impossible to make any satisfactory conclusions from this data without statistical analysis, which can be found in Section 6.3.5. It is believed that M38 maintains impact energy to a higher degree in relation to the S sample as a result of the GF content being more similar to that of S (Figure 19).

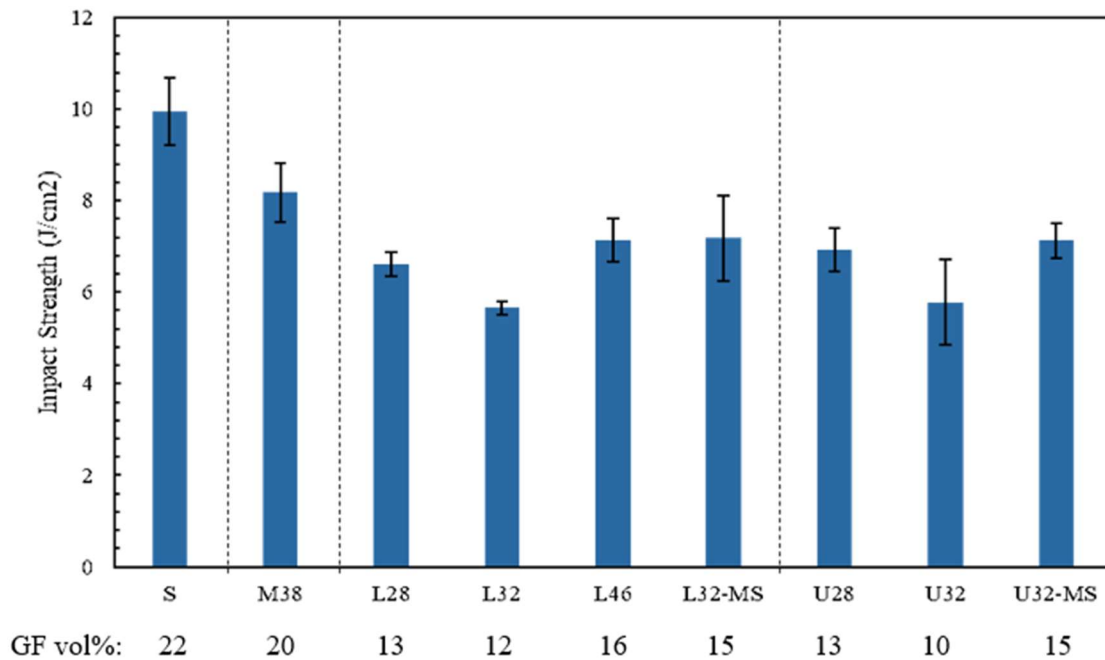


Figure 19: Impact energy of SMC composites.

4.4 Ashby Plot

Ashby plots have been used in literature to plot different mechanical properties on the x- and y-axes, such as specific tensile strength versus specific Young's modulus. Various families of materials, shown in separate colors, are then compared based on these characteristics [35]. The Ashby plots in Figure 20 and Figure 21 provide contextualization for the results of this study by benchmarking the specific tensile (Figure 20) and specific flexural (Figure 21) properties against other polymer composite systems found in literature. Although the comparisons are not ideal, it gives an understanding of how the mechanical results in this study compare to similar formulations and the current state of the art (Table 15). These papers were used for comparison to the present study since most of them utilized the SMC process. C was made using hand lay-up, but this is also a common manufacturing process for GF reinforced composites. The papers plotted in Figures 20 and 21 also compared both standard density composites and reinforced syntactic foams. Thus, it is possible to see how the properties from this study compare to standard and lightweight composites.

Table 15: Mechanical properties benchmarking from literature for Ashby Plot (Figure 20 & 21).

Sample	Manufacturing Method	Syntactic Foam	Fiber Type	Citation
This Study	SMC	yes	Glass	This Study
A	SMC	no	Glass	[2]
B	SMC	no	Basalt	[36]
C	Hand Layup	no	Natural	[38]
D	SMC	yes	Glass	[11]
E	SMC	yes	Glass	[33], [37]

Figure 20 shows that the tensile results of this study are comparable to those found in literature [11,33,36–39]. Furthermore, the specific tensile modulus was higher than that reported in Devi 1996 but lower than that of the IDI Composites, whereas the specific strength was comparable to results reported elsewhere (Figure 20) [11,33,36–39]. The specific flexural properties (Figure 21) are also comparable to the corresponding properties reported in literature [33,37,39]. Similar to the tensile properties, the IDI Composites exhibit superior specific flexural properties [33,37].

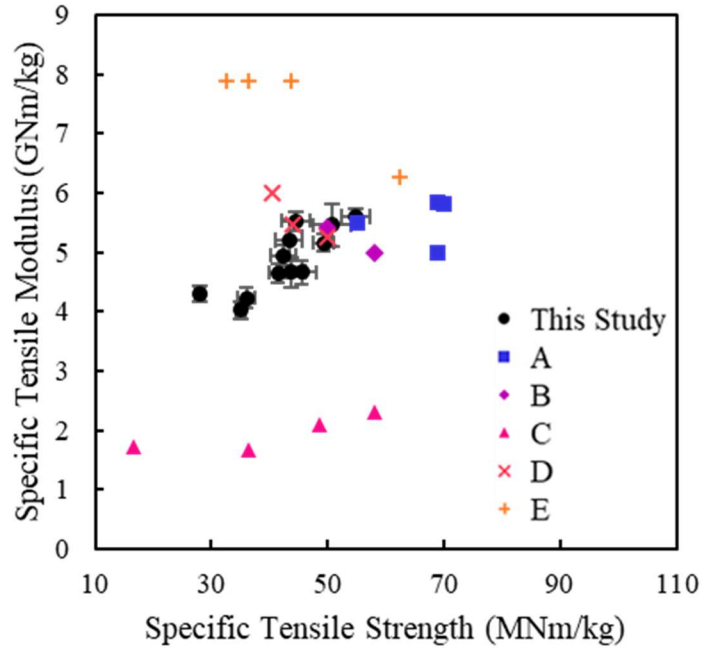


Figure 20: Ashby Plot of specific tensile properties comparing this study with results [11,32,35-38] on SMC composites and fiber reinforced syntactic foams. See Table 5 for definitions of A, B, C, D, and E.

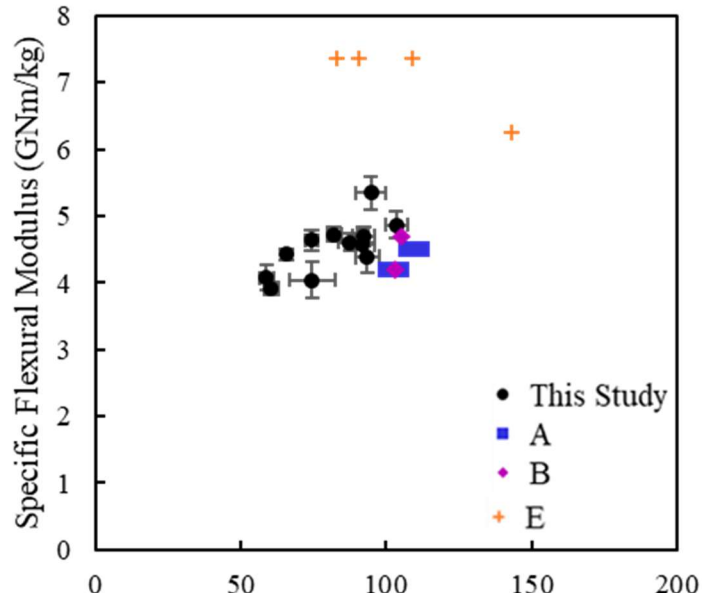


Figure 21: Ashby Plot of specific flexural properties comparing this study with results [32,36,38] on SMC composites and fiber reinforced syntactic foams. See Table 5 for definitions of A, B, and E.

The differences observed are expected considering that the various studies used for the comparison did not necessarily use the same materials. Additionally, the pressure used during compression molding in this study was lower than the one recommended by the resin supplier, and thus it is expected that the mechanical properties obtained are not the maximum possible.

4.5 Chapter Summary

An overview of the tensile, flexural, and impact properties for all formulations produced was provided. Formulations must have equivalent GF content to compare within the data set for each mechanical property. Due to the large standard deviations of most formulations, no significant conclusions can be made without statistical analysis, which will be explored in Chapter 6.

Chapter 4 also showed that in the current study, only S, M38, and L46 met the industry standard for tensile strength. No formulations achieved the desired tensile modulus, flexural strength, or flexural modulus values. This was most likely due to limitations in the maximum pressure that could be applied with this study's equipment. Despite this, the Ashby plots demonstrated that the data found here was comparable with other academic findings. The next chapter will discuss potential mechanisms that could affect the mechanical properties of different formulations.

CHAPTER 5. POTENTIAL REINFORCING MECHANISMS AND COUNTERACTING PHENOMENA

In this chapter, the potential mechanisms that could affect the mechanical behavior of these complex composites and any counteracting phenomena will be discussed. The likelihood of these mechanisms will then be explored using JMP statistical analysis in the following chapter.

5.1 Independent Variables and Corresponding Reinforcing Mechanisms

The independent variables that will be explored in the statistical analysis are: GF vol%, HGS vol%, density, diameter, and surface modification, as well as CaCO₃ vol% (Table 16). Each, or a combination, of these variables could contribute to the mechanical behavior of these complex reinforced syntactic foams. GF acts as the reinforcing phase in the composites. However, the variation in the GF content due to inherent randomness in the SMC process could mask any effect of other variables. The following mechanisms influencing tensile properties have been discussed in literature: Low volume content of HGS in the composite is preferred as there is relatively more resin paste for wetting of the fillers and GF and thus these composites may exhibit higher tensile properties compared to those containing higher content of HGS. It has also been reported that HGS may act as stress concentrators [40]. According to experimental studies and theoretical micromechanical models used to describe the tensile modulus of syntactic foams, the modulus was found to either increase or decrease with increasing HGS content [41–43]. The response is dependent upon the HGS properties including strength and radius ratio. If

the HGS replace higher performance matrix polymer, the modulus will decrease. Conversely, if high strength HGS replace a relatively weak polymer or filler, the syntactic foam modulus will increase [41].

In a hybrid syntactic foam, maintaining a strong interface between the polymer and the HGS filler is of importance because if there is separation, a void could form in this area and act as a stress concentration point. As reported, tensile fracture often occurs due to the debonding of the particle-matrix interface, thus it follows that a stronger interfacial bond due to the silane surface treatment would increase tensile properties [44]. It has been reported that the tensile modulus increased as silane treated HGS content increased up to 20 vol% in polypropylene syntactic foams [45].

The effect of surface functionalization on the flexural properties has also been studied. Surface functionalization is expected to have a positive effect on flexural strength, as this property strongly relates to the ability to transfer load along an interface. This ability improves with surface functionalization [46,47]. Strong HGS-matrix bonding can prevent crack initiation, which is most likely to occur on the tensile side of the composite coupons during the three point bending, and crack propagation [47,48]. Literature has shown that HGS functionalized with methacryloxypropyl trimethoxysilane have a 10% greater flexural strength and 5% greater flexural modulus than uncoated HGS in a UPR matrix composite [4]. Furthermore, Tagliavia, et al. showed that when a 0.32 g/cm³ HGS replaced vinyl ester, in unreinforced syntactic foams, the flexural modulus generally decreased. Although there is no significant difference when increasing from 40 to 50 vol%, the modulus decreases once more at 60 vol%. Additionally, there appears to be no saturation point of this property [46]. Lastly, Ferreira, et al. found that flexural modulus decreased

with increasing HGS content from 0 to 50 vol% in an unreinforced syntactic foam. When GF between 0 and 1.2 vol% were added to the syntactic foam, there was still a decrease in flexural stiffness when increasing from 10 to 43 vol% HGS. As expected, the addition of such a small amount of GF does not significantly increase the properties at 43 vol% HGS [49].

Mechanisms that affect impact properties of syntactic foams are discussed next. Impact energy has a drop with the inclusion of even a small amount of HGS, as in the mid-density sample. Despite this, the values stabilize across mid, low-, and ultra-low densities and for all types of HGS, as presented in Figure 19. Literature has indicated that impact is adversely affected by any type of HGS and is independent of loading [50,51]. This phenomenon has been attributed to HGS acting as stress concentration points and restricting the plastic flow of the polymer [50].

Table 16: Potential mechanisms of each composite variable that could affect the mechanical properties.

Variables	Potential Mechanism
GF vol%	Reinforcement phase
HGS vol%	Replacement of stronger phase with weaker phase Agglomeration of HGS Stress concentration Less resin for wetting of GF and fillers Crack initiation at interface with resin
HGS Density	Affects HGS wall thickness
HGS Diameter	Determines size of inclusion in composite Affects HGS wall thickness
Surface Modification	Improved dispersion of HGS Improved interaction between HGS and resin
CaCO ₃ vol%	Improves properties compared to HGS Less significant stress concentration point

5.2 Chapter Summary

Chapter 5 laid out the independent variables and the mechanisms that could possibly affect the properties of the composites. The next chapter will attempt to determine the significance of the effect of each of these variables on each mechanical property.

CHAPTER 6. JMP STATISTICAL ANALYSIS

In this chapter the author discusses how an ideal DOE for all formulations should look. This includes both a full-factorial design and a mixed-level fractional factorial. Next, the number of formulations studied are limited to those that more closely align with a full-factorial, fractional factorial, or Taguchi array and the corresponding mechanical properties are discussed in that context and analyzed using the JMP software.

6.1.1 All Formulations

All formulations (Table 7), excluding the standard density baseline, tested in this study were made into “correct” DOEs utilizing the JMP software. These DOEs were then compared to our sample set to determine if they met the requirements for satisfactory statistical analysis. Although many variables were considered when the reinforcing mechanisms were discussed, only three were completely independent of one another: HGS density, surface modification, and HGS content. HGS density is dependent on diameter. Furthermore, the HGS content is indicative of whether the composite is mid-, low-, or ultra-low density, which also determines the GF content. As a result, GF content was not considered in these DOE arrays. The first DOE was a full-factorial with all combinations of the factors’ levels (Table 17).

Table 17: Full-factorial DOE of all formulations that include HGS. Yellow highlight indicates which runs were completed in the present study.

Run	HGS Density (g/cm ³)	Surface Modification	HGS Content	Formulation
1	0.28	0	19	
2	0.28	0	32	L28
3	0.28	0	43	U28
4	0.32	0	19	
5	0.32	0	32	L32
6	0.32	0	43	U32
7	0.38	0	19	M38
8	0.38	0	32	
9	0.38	0	43	
10	0.46	0	19	
11	0.46	0	32	L46
12	0.46	0	43	
13	0.28	1	19	
14	0.28	1	32	
15	0.28	1	43	
16	0.32	1	19	
17	0.32	1	32	L32-MS
18	0.32	1	43	U32-MS
19	0.38	1	19	
20	0.38	1	32	
21	0.38	1	43	
22	0.46	1	19	
23	0.46	1	32	
24	0.46	1	43	

The yellow highlighting in Table 17 indicates which sample combination matches an existing formulation from this study. Only 33% of this full-factorial DOE was completed. Any run that required a surface functionalized version of a HGS, other than 32, (Runs 13-15 and 19-24) could not be completed, as this type of sphere did not exist.

As a result, a mixed-level fractional factorial was created to determine if the samples investigated met the requirements for that type of DOE (Table 18) [52]. A mixed-level fractional factorial was necessary because surface modification has two levels (0 and 1, or “no” and “yes”), HGS content has three levels (19, 32, 43 vol%), and HGS density has 4 levels (0.28, 0.32, 0.38, and 0.46 g/cm³). Only 42% of the fractional factorial was completed, so it was also insufficient for statistical analysis.

Table 18: Mixed-level fractional factorial of all samples that include HGS [51].

Run	HGS Density (g/cm ³)	Surface Modification	HGS Content	Formulation
1	0.28	0	19	
2	0.32	0	19	
3	0.38	0	19	M38
4	0.46	0	19	
5	0.28	0	32	L28
6	0.32	0	32	L32
7	0.38	1	32	
8	0.46	1	32	
9	0.28	1	43	U28-MS
10	0.32	1	43	U32-MS
11	0.38	1	43	
12	0.46	1	43	

6.2 Select Formulations

Formulations were then limited to L28, L32, L32-MS, U28, U32, and U32-MS in an attempt to find a DOE that was completed within the formulations that were investigated.

Table 19 has the details of these syntactic foam formulations. Wall thickness (μm) was not considered as a factor because the values were comparable for all six samples.

Table 19: Input variables for JMP software for six formulations of interest.

Name	HGS Density (g/cm^3)	Outer Diameter (μm)	HGS Loading (vol%)	Surface Functionalization	GF Loading (vol%)	CaCO₃ Loading (vol%)
L28	0.28	30	33	N	13	4.5
U28	0.28	30	43	N	13	0
L32	0.32	25	35	N	12	4.5
U32	0.32	25	44	N	10	0
L32-MS	0.32	25	34	Y	15	4.5
U32-MS	0.32	25	42	Y	15	0

Table 20 lays out the full-factorial for these six formulations. In this case, 75% of the runs had been completed. Again, runs 3 and 4 were not possible as there was not a surface modified HGS 28.

Table 20: Full-factorial of six formulations shown in Table 19. Yellow highlight indicates which runs have been completed in this research.

Run	HGS Density (g/cm ³)	Surface Modification	HGS Content	Formulation
1	0.28	0	32	L28
2	0.28	0	43	U28
3	0.28	1	32	
4	0.28	1	43	
5	0.32	0	32	L32
6	0.32	0	43	U32
7	0.32	1	32	L32-MS
8	0.32	1	43	U32-MS

For comparison, a fractional factorial was produced using the factor and level combinations shown in Figure 22. It was found that a fractional factorial and Taguchi array are the same for a study with three parameters and two levels each (Table 21). As before, only 75% was completed, and Run 2 was not possible with the available HGS types.

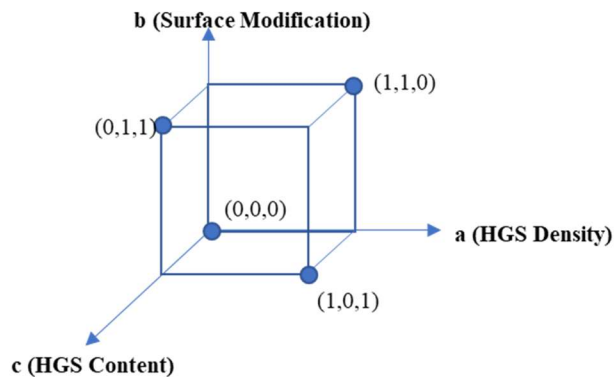


Figure 22: Schematic showing factor and level combinations used in a fractional factorial DOE.

Table 21: Fractional factorial DOE for formulations found in Table 19. This is an identical DOE to Taguchi Orthogonal Array for the same set of inputs.

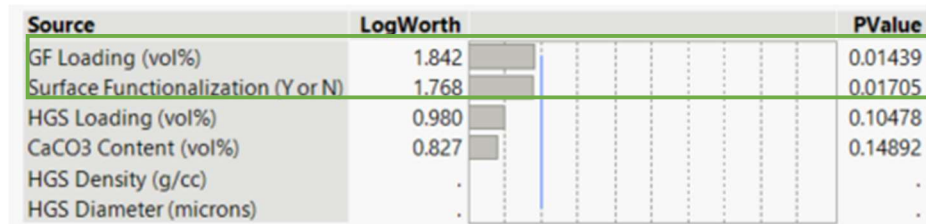
Run	HGS Density (g/cm ³)	Surface Modification	HGS Content	Formulation
1	0.28	0	32	L28
2	0.28	1	43	
3	0.32	0	43	U32
4	0.32	1	32	U32-MS

6.3 JMP Analysis of Mechanical Properties

Statistical analysis using the full-factorial of the limited sample set (Table 20) for various mechanical properties is detailed below. The JMP software was used to try to determine which input variables had a significant effect on the desired mechanical output. The interaction of these factors was not able to be investigated, so this analysis is not representative of a true SMC syntactic foam. In each formulation, most of the variables were changing simultaneously, so the JMP software had to deconvolute these effects. Consequently, the results may not be statistically significant and may not be able to be used to extrapolate understanding of formulations outside of this incomplete design space. The input values are outlined in Table 19. The JMP analysis produced two types of analysis outcomes. The first, such as Figure 23, is the significance of each input variable on a particular mechanical property. The second, for example in Figure 24, is a comparison to determine if the resulting mechanical property for each formulation is significantly statistically different. A p-value tells the user how strong the evidence is that the average of two samples are statistically different. Any p-Value below 0.05 is considered significant. LogWorth is another representation of the p-value, but it is not relevant in this discussion.

6.3.1 Tensile Strength

Statistical analysis was completed using the tensile results for the six formulations. Figure 23 was a result from the JMP software analysis and shows which input variables have p-values of less than 0.05. These are the factors that significantly affect the tensile strength. It was found that the two most influential factors are GF loading (vol%) and surface functionalization. As expected, the GF content has the most influence on tensile strength, as it is the reinforcing phase. The statistical significance of surface functionalization suggests that, as stated in Table 16, the sphere modification may be improving dispersion of the HGS or interaction between the HGS and matrix.



Source	LogWorth	PValue
GF Loading (vol%)	1.842	0.01439
Surface Functionalization (Y or N)	1.768	0.01705
HGS Loading (vol%)	0.980	0.10478
CaCO3 Content (vol%)	0.827	0.14892
HGS Density (g/cc)	.	.
HGS Diameter (microns)	.	.

Figure 23: JMP results for significant input variables that affect tensile strength.

A statistical comparison between all the samples was completed and can be seen in Figure 24. Two formulations result in significantly different tensile strength if their comparison results in a p-value of less than 0.05. This demonstrates that at low HGS loadings (i.e., low-density formulations), there is no significant difference in tensile strength. In addition, when comparing low- and ultra-low sample, it is seen that there is only a significant difference between L32 and U32. All other HGS types maintain their tensile strength at both loadings. This could be an artifact of the influence of the GF loading

on this property, as the samples with HGS 32 have the lowest GF values. The steep drop of the tensile strength for HGS 32 in Figure 25.

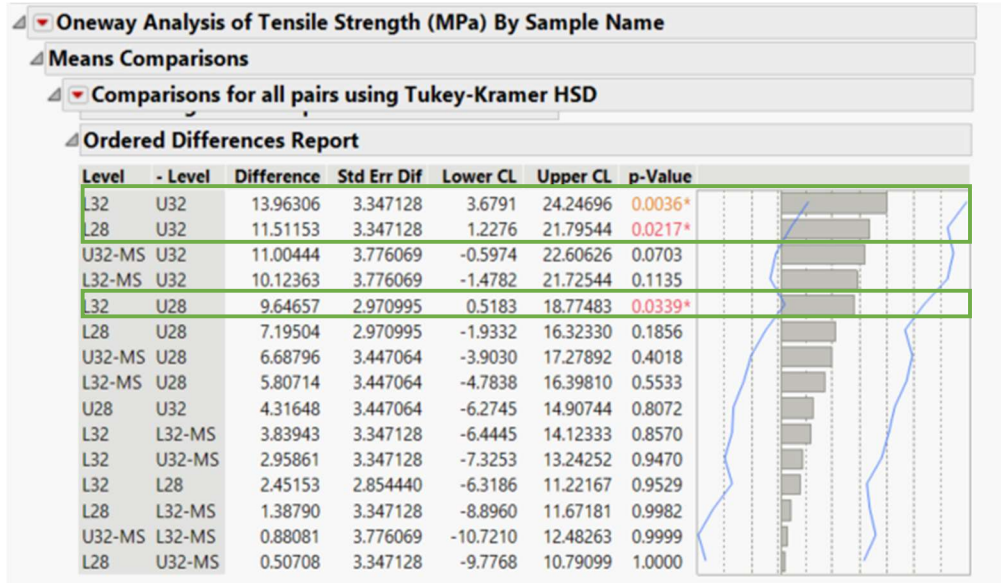


Figure 24: JMP statistical comparison for tensile strength between the six formulations of interest.

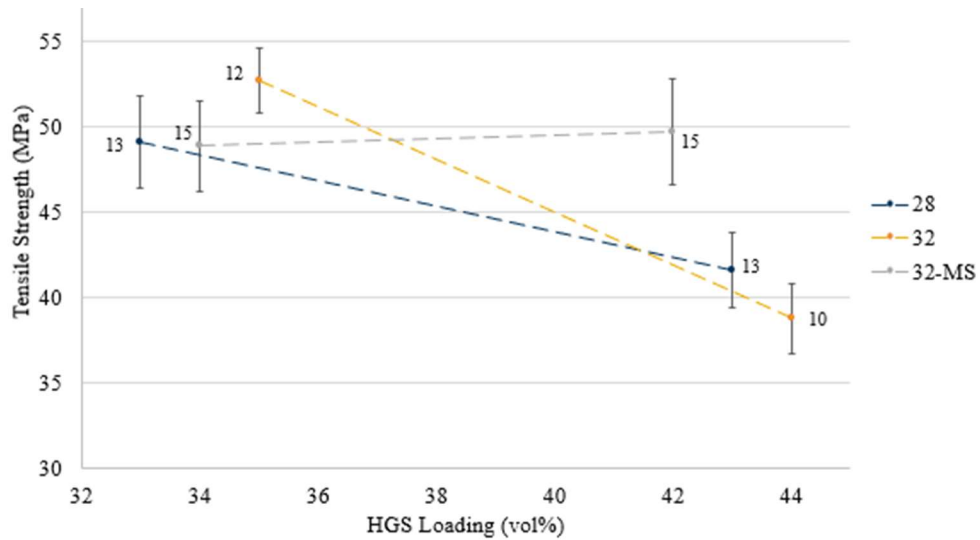


Figure 25: Tensile strength (MPa) vs. HGS loading (vol%) of three sphere types.

6.3.2 Tensile Modulus

The effect of these variables on tensile modulus was also investigated. In this case, it was determined that GF loading was the only significant factor, within this set of experiments, influencing the tensile modulus (Figure 26). Again, this is expected, as GF is the reinforcement in these composites.

Source	LogWorth	PValue
GF Loading (vol%)	1.377	0.04195
Surface Functionalization (Y or N)	1.050	0.08909
CaCO ₃ Content (vol%)	0.111	0.77473
HGS Loading (vol%)	0.105	0.78481
HGS Density (g/cc)	.	.
HGS Diameter (microns)	.	.

Figure 26: JMP results for significant input variables that affect tensile modulus.

It is evident from Figure 27 that no two samples' tensile moduli are significantly different. As a result, within the error of this study, the replacement of CaCO₃ with HGS does not matter with respect to this particular mechanical property.

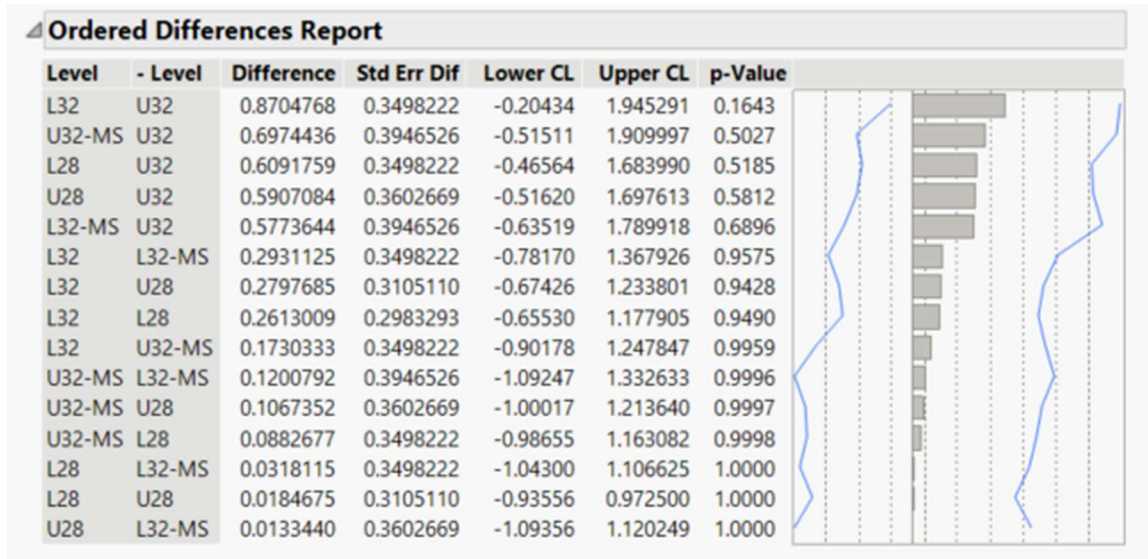


Figure 27: JMP statistical comparison for tensile modulus between six formulations of interest.

6.3.3 Flexural Strength

Flexural strength statistical analysis resulted in an interesting outcome. Figure 28 shows that there is no significant effect of any of the input variables. However, Figure 29 makes it clear that there is a significant decrease in the flexural strength between L28 and U28. Additionally, HGS 32 and 32-MS maintain their flexural strength even with increasing HGS content.

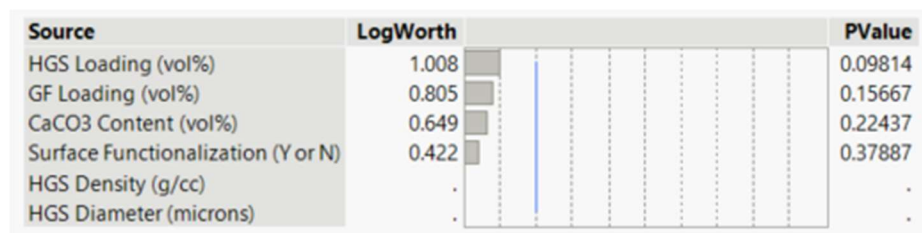


Figure 28: JMP results for significant input variables that affect flexural strength.

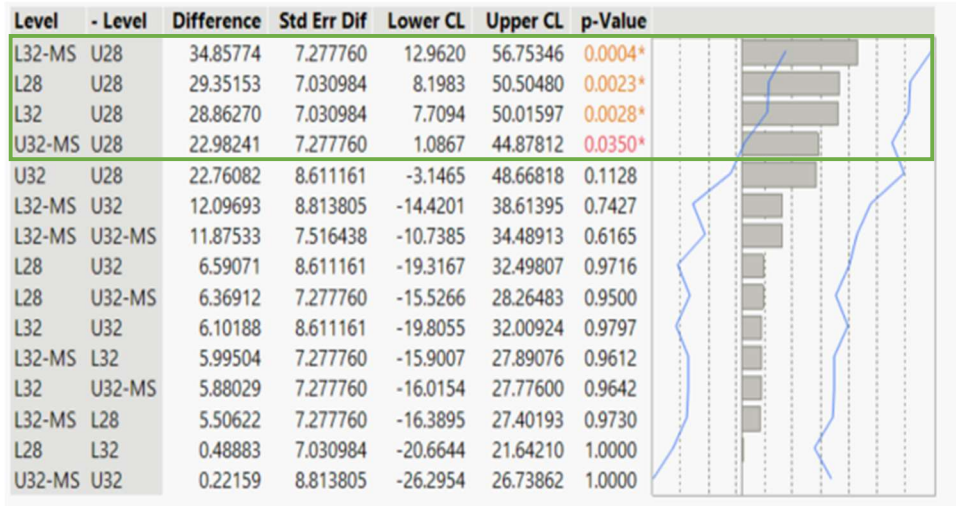


Figure 29: JMP statistical comparison for flexural strength between six formulations of interest.

In Figure 30, one can see that U28 is significantly lower than other samples. Because there is no obvious cause for this significant decrease in the properties of U28 from the factors considered, it could be due to other origins not considered in Figure 28. One possibility is poor surface finish on the final plate for this formulation. Another potential cause is inconsistent distribution of GF in the composite causing weaker regions from where the test coupons were cut.

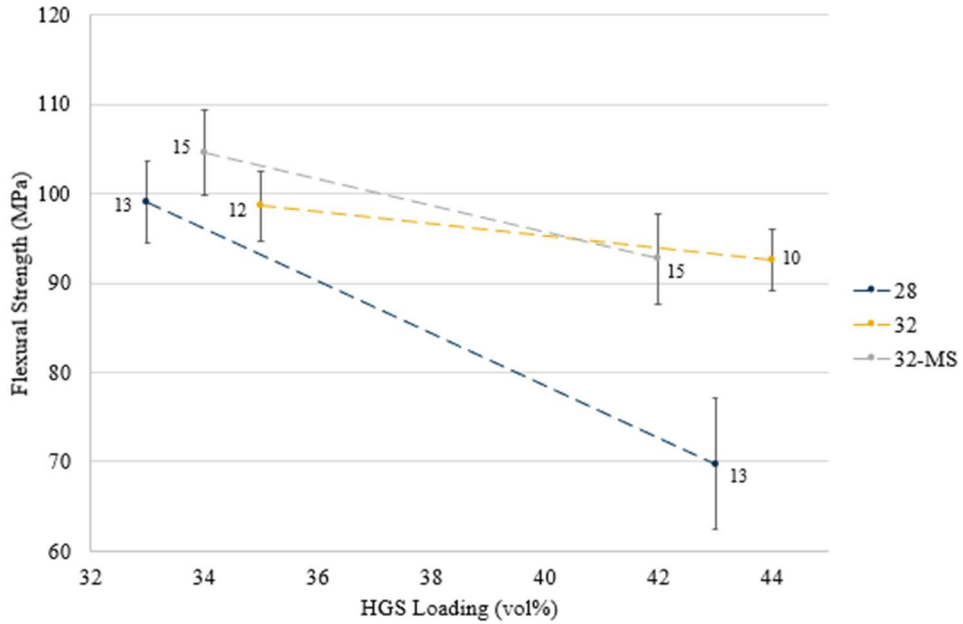


Figure 30: Flexural strength (MPa) versus HGS loading (vol%) of three sphere types.

6.3.4 Flexural Modulus

Flexural modulus as a function of the variables in Figure 31 was also investigated. In this case, it was determined that HGS loading and CaCO₃ content were the two significant factors. It is noteworthy that GF content apparently does not affect the flexural modulus. Because flexural modulus is an out-of-plane property, HGS and CaCO₃ may dominate this property over GF, within the scope of this study.

Source	LogWorth	PValue
HGS Loading (vol%)	2.792	0.00161
CaCO ₃ Content (vol%)	2.493	0.00322
Surface Functionalization (Y or N)	0.733	0.18491
GF Loading (vol%)	0.248	0.56441
HGS Density (g/cc)	.	.
HGS Diameter (microns)	.	.

Figure 31: JMP results for significant input variables that affect flexural modulus.

Figure 32 shows that flexural modulus decreases from L28 to U28. Interestingly, Figure 32 shows that only HGS 28 demonstrates a drop in flexural modulus between low- and ultra-low density formulations. This implies that lower quantities of calcium carbonate or higher HGS loadings adversely affect flexural modulus. However, this is not seen for HGS 32 or 32-MS, which have the same changes in HGS and CaCO₃ content when changing density. Consequently, the lower U28 values could once again, be attributed to outside factors, such as surface finish or inconsistent GF loading within the composite plate.

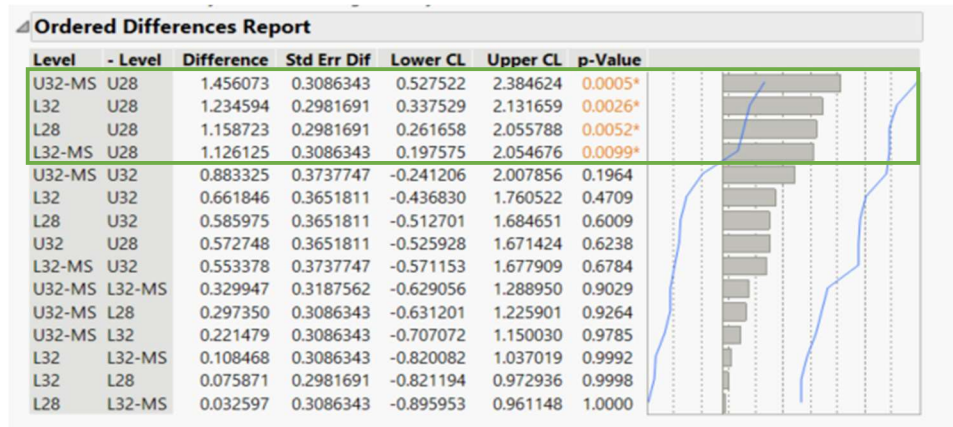


Figure 32: JMP statistical comparison for flexural modulus between six formulations of interest.

Figure 33 shows that all low-density samples have essentially equivalent flexural moduli. This aligns with the results in Figure 32. Although it appears that U32 is statistically different from L32, it is not actually the case. HGS 32 and 32-MS maintain their flexural moduli regardless of loading.

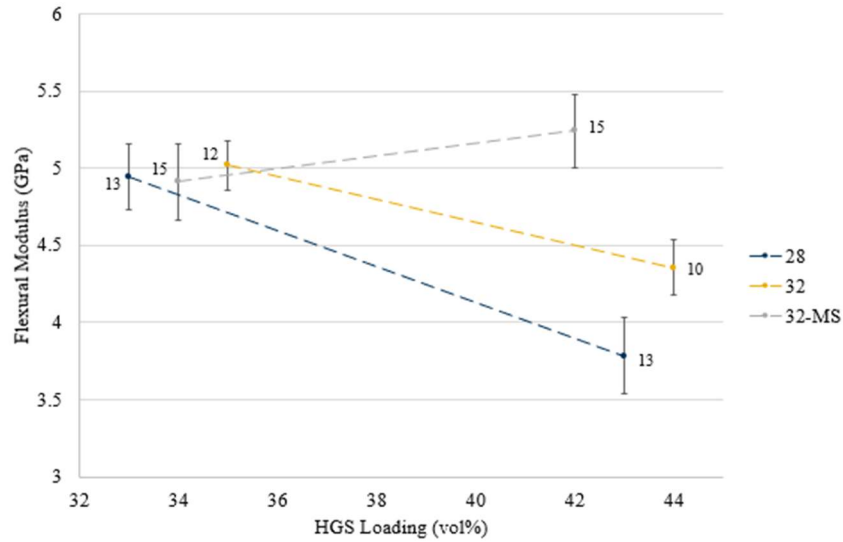


Figure 33: Flexural modulus (GPa) versus HGS content (vol%) for spheres 28, 32, and 32-MS.

6.3.5 Impact Properties

Figure 34 indicates that none of the input variables considered significantly affect the impact energy.

Source	LogWorth	PValue
Surface Functionalization (Y or N)	0.319	0.48010
HGS Loading (vol%)	0.117	0.76324
CaCO3 Content (vol%)	0.105	0.78567
GF Loading (vol%)	0.005	0.98917
HGS Density (g/cc)	.	.
HGS Diameter (microns)	.	.

Figure 34: JMP results for significant input variables that affect impact energy.

Figures 35 and 36 show that for spheres 28, 32, and 32-MS, there is no effect on impact energy from different HGS loadings. Additionally, there is no significant difference in the resulting impact energy across HGS types. Essentially, impact property is not affected by HGS type or loading. This aligns with the literature discussed in Section 5.1

and with the results from Figure 34 that no HGS property significantly influences this property's outcome.

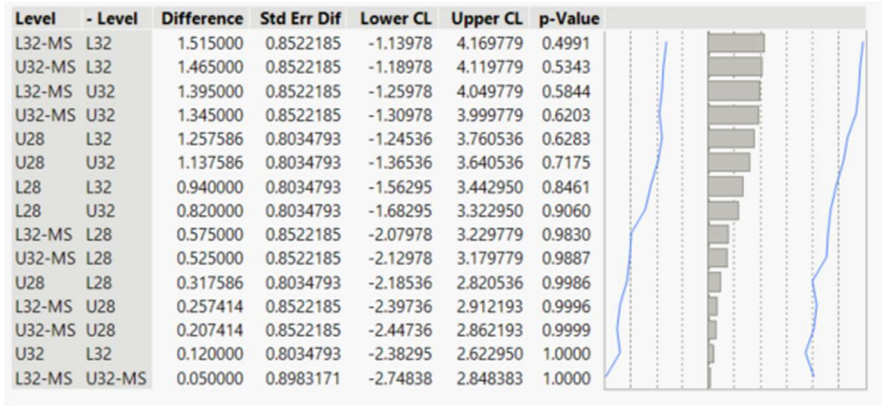


Figure 35: JMP statistical comparison for impact energy between six formulations of interest.

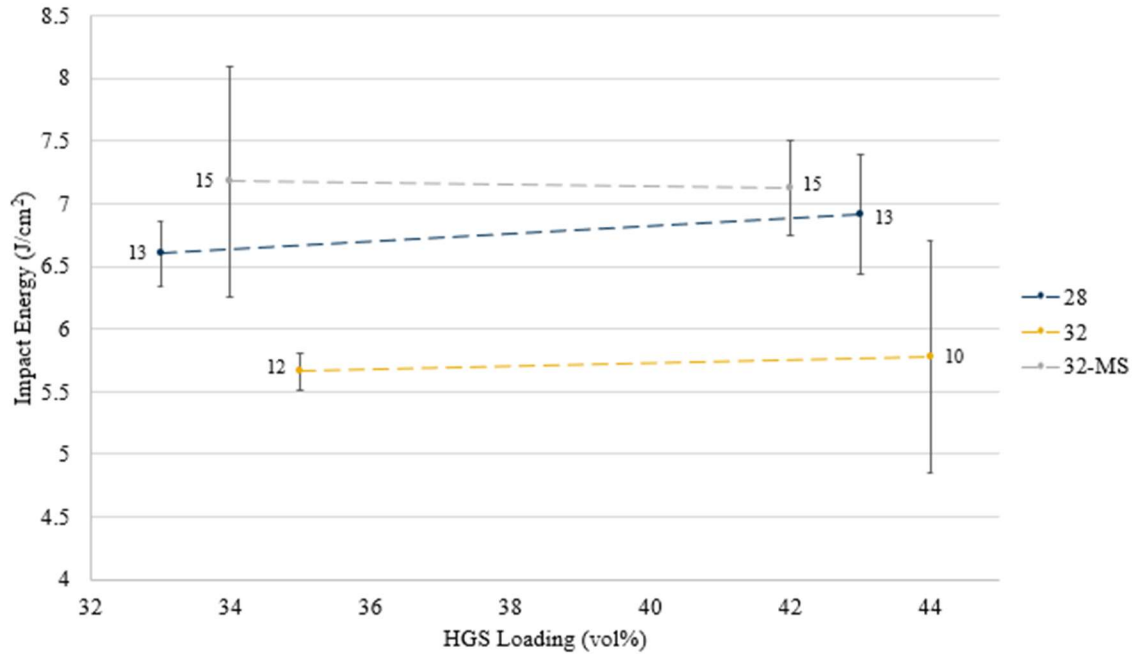


Figure 36: Impact Energy (J/cm²) versus HGS loading (vol%) for three HGS types.

6.4 Chapter Summary

A summary of the significant variables affecting each mechanical property found via JMP statistical software is provided in Table 22. It was found that, as expected, GF loading dominates tensile strength and modulus, most likely because these are in-plane properties. However, flexural modulus was more influenced by HGS and CaCO₃ content. Flexural strength and impact energy were not statistically shown to be affected by any of the considered variables. Though, any differences shown in these two properties between the samples could be due to other defects or inconsistencies in the composite plates. A contour plot comparing statistically significant variables and their effect on the corresponding mechanical property can be found in Appendix A.

Table 22: Summary of statistically significant variables affecting the mechanical properties of SMC fiber reinforced syntactic foam composites.

	Tensile Strength (MPa)	Tensile Modulus (GPa)	Flexural Strength (MPa)	Flexural Modulus (GPa)	Impact Energy (J/cm²)
#1	GF Loading (vol%)	GF Loading (vol%)	-	HGS Loading (vol%)	-
#2	Surface Functionalization	-	-	CaCO ₃ Content (vol%)	-
#3	-	-	-	-	-
#4	-	-	-	-	-
#5	-	-	-	-	-

U28 was found to have the lowest properties for flexural strength and modulus. Though most samples showed no significant difference and, thus, maintained their properties between their low- and ultra-low density formulations. Since no formulations

were shown to be superior to others, the next step is to compare their costs of production, which is examined in the next chapter.

CHAPTER 7. COST ANALYSIS AND SUGGESTIONS FOR MANUFACTURERS

The following chapter is comprised of a cost comparison of all formulations made. In the previous chapter, it was found that no statistically significant conclusions could be made within the bounds of the limited set of samples that was analyzed. In other words, within the confines of this study, adding HGS made no significant difference to any properties. Additionally, no HGS type and loading combination was found to provide superior properties compared to other syntactic foam formulations. As a result, manufacturers should aim to make these samples as inexpensive as possible. A cost analysis was performed for all nine formulations to determine the one that is most cost-effective for industrial scale production.

7.1 Formulation Cost Comparison

A cost estimate was completed for each formulation in Table 23. Each mass unit (kg) is a part per hundred (phr) resin. In other words, for every 100 kg of combined Arotran 774 and 775, there will be a certain mass in kilograms of the other components. For all formulations, the processing path and equipment costs are essentially equivalent. Therefore, capital investment and labor costs were negligible when assessing the manufacturing cost. This analysis was solely dependent upon materials.

The most expensive component of the formulations is the HGS. All types are more expensive than both types of resin, Arotran 774 and 775, as well as the glass fiber. In a typical SMC standard density composite, CaCO_3 is added to the resin paste to increase

volume with a low-cost alternative to the polyester resin. However, in the syntactic foam formulations, the inexpensive calcium carbonate (\$0.14/kg) is replaced with HGS of price ranging from \$13.10-\$23.90/kg. As a result, the HGS used to make the syntactic foams are the driving force behind the formulation costs. Thus, it is reasonable that S is the least expensive formulation, when considering the major resin paste elements. However, within the six formulations that were statistically analyzed, L28 was the most cost-effective (though still approximately \$293 more expensive than standard density). Although, the more expensive production cost of L28 SMC composites may be worth it, depending on the applications and customer needs.

Table 23: Material-driven cost analysis of all formulations studied in this research.

Material	Cost/kg	Mass Used (kg)									
		S	M38	L28	L32	L46	L32-MS	U28	U32	U32-MS	
Arotran 774	\$4.85	70	70	70	70	70	70	70	70	70	70
Arotran 775	\$3.86	30	30	30	30	30	30	30	30	30	30
CaCO ₃	\$0.14	305.18	99.14	27.34	28.36	9.67	28.36	-	-	-	-
28	\$23.46	-	-	19.32	-	-	-	26.99	-	-	-
32	\$23.90	-	-	-	24.12	-	-	-	31.39	-	-
HGS 38	\$20.46	-	16.88	-	-	-	-	-	-	-	-
46	\$13.10	-	-	-	-	39.05	-	-	-	-	-
32-MS	\$23.90	-	-	-	-	-	24.12	-	-	-	31.39
GF	\$2.00	173.49	126.78	112.98	117.19	114.47	117.19	100.24	95.90	95.90	95.90
Total Cost		\$845.01	\$1068.10	\$1138.33	\$1270.12	\$1197.15	\$1270.12	\$1288.97	\$1397.32	\$1397.32	\$1397.32

7.2 Suggestions for Manufacturers

Within the experimental error and scope of this research, all variables are confounding. This was a limited set of data, and the DOE was not set up in such a way that the JMP software could delineate the model. It was only definitively shown that U28 had significantly lower flexural strength and flexural modulus than L28. Consequently, it is unsatisfactory to extrapolate the effect of different filler loadings outside of this design space. The main take away for future manufacturers referencing this data set is to focus on the effect of the components on the overall cost to produce each formulation. Within this study, it was found that S is the least expensive formulation to produce. However, L28 was the least expensive within the statistically analyzed samples. Because they have no significantly different properties than other formulations, it is the best choices for manufacturers who aim to make lightweight glass fiber reinforced SMC composites for automotive applications.

7.3 Chapter Summary

A cost analysis for all formulations was discussed in Chapter 7. The estimation was highly dependent upon the material costs. Based on this, S and L28 were the most cost-effective formulations. L28 was suggested for future manufacturers as the superior composite choices from this study, as they were the least expensive to produce and showed no significant decrease in properties. The next chapter will detail a study into the effect of CaCO_3 and HGS on water uptake of reinforced syntactic foams.

CHAPTER 8. WATER UPTAKE

During use as an exterior autobody panel, SMC composites can absorb moisture either through humidity or direct contact with water. Exposure to water has the potential to compromise the durability and mechanical properties of the composite [20]. Thus, the water uptake of lightweight SMC compared to that of standard density is an important aspect of degradation that must be understood. This chapter compares the water uptake of three samples S, M38, and L46. Possible mechanisms that could explain the disparity in water uptake are discussed. These include the effect of glass surface area, calcium carbonate surface area, the relative hydrophilicity of the components, and a potential steric effect.

8.1 Effect of Formulation on Water Uptake

Samples of S, M38, and L46, were submerged in 70°C DIW and measured periodically to understand the effect of the formulation on water absorption behavior. It is evident that this is not a direct comparison because M38 and L46 use different HGS types with varying properties. However, this is necessary because low-density samples were not produced with the 38 sphere. Figure 37 shows that standard density samples absorbed the least amount of DIW and had very small standard deviations across samples on a particular time interval. This figure also revealed that the mid-density samples had greater water uptake than the standard density. However, the most substantial moisture weight gain occurred in the low-density samples. The shoulder seen in 46 been shown to occur in only high absorption samples in existing literature [53,54].

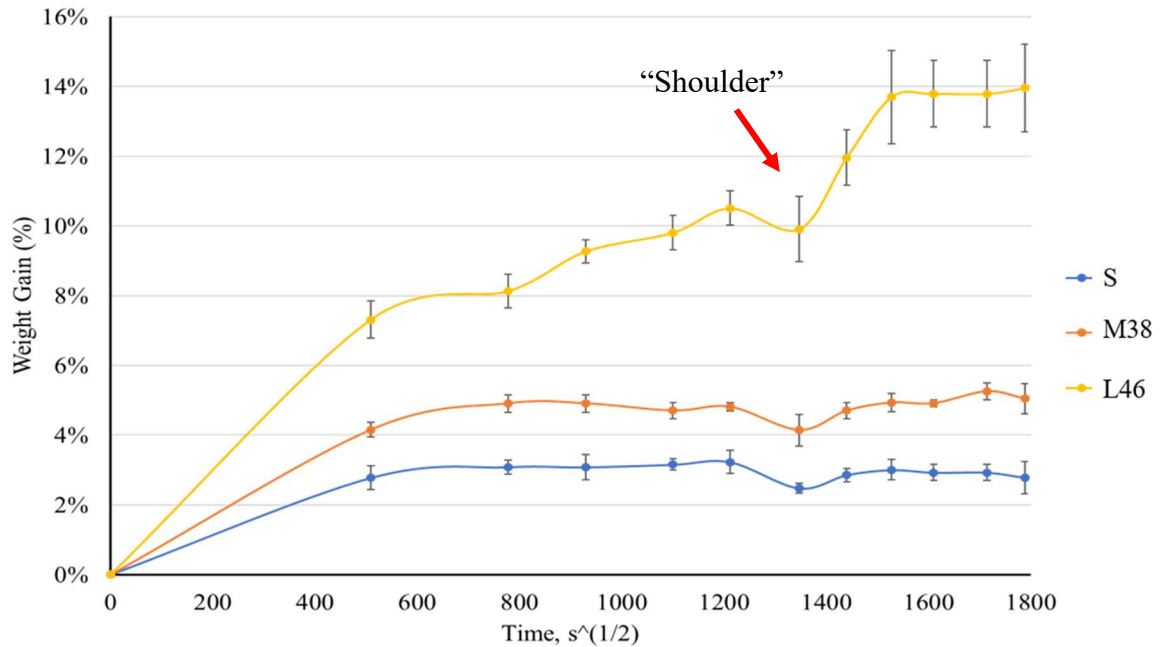


Figure 37: Weight Gain (%) vs. Time (s^(1/2)) of samples immersed in DIW at 70°C.

8.1.1 Effect of Glass Surface Area on Water Uptake

The three composite components that would contribute most to water uptake due to their high-volume fraction and hydrophilicity are: GF, HGS, and CaCO₃. Figure 38 shows the total surface area of GF and HGS in the formulations S, M38, and L46 at a volume of 2.4 L. It was intended that as the composite density decreases from 1.9 g/cm³ to 1.5 g/cm³, and 1.2 g/cm³, the GF surface area would stay constant as the target was to maintain 20 vol% GF. However, this was not achieved due to the inherent randomness in the SMC line, resulting in a lower GF content in case of L46. On the other hand, it is evident that as composite density decreases, HGS surface area increases. This corresponds to the greater HGS content as a filler to replace CaCO₃ in lower density formulations. The GF and HGS surface areas in Figure 38 can be compared to the total steady-state weight gain percent (%) from water uptake shown in Figure 39. The steady-state weight gain

increases as HGS surface area increases, while GF surface area remains mostly constant. As spheres are added, the total glass surface area of the composite will become significantly larger. This leads to greater water absorption as glass is hydrophilic and the addition of HGS creates more interfaces with the resin into which moisture can be stored.

HGS 46 has the highest density of all the sphere varieties. Therefore, in order to achieve the low-density formulation target, more HGS must be added to the formulation. This resulted in the greater increase in the HGS total surface area and steady-state water absorption from M38 to L46, compared to the lesser increase from S to M38. The steady state weight gain increased by 2.33 percentage points from S to M38 when HGS surface area increased by $5.07 \times 10^5 \text{ cm}^2$. From M38 to L46, the steady-state weight percent increased by 8.53 percentage points when HGS surface area increased by $1.23 \times 10^6 \text{ cm}^2$.

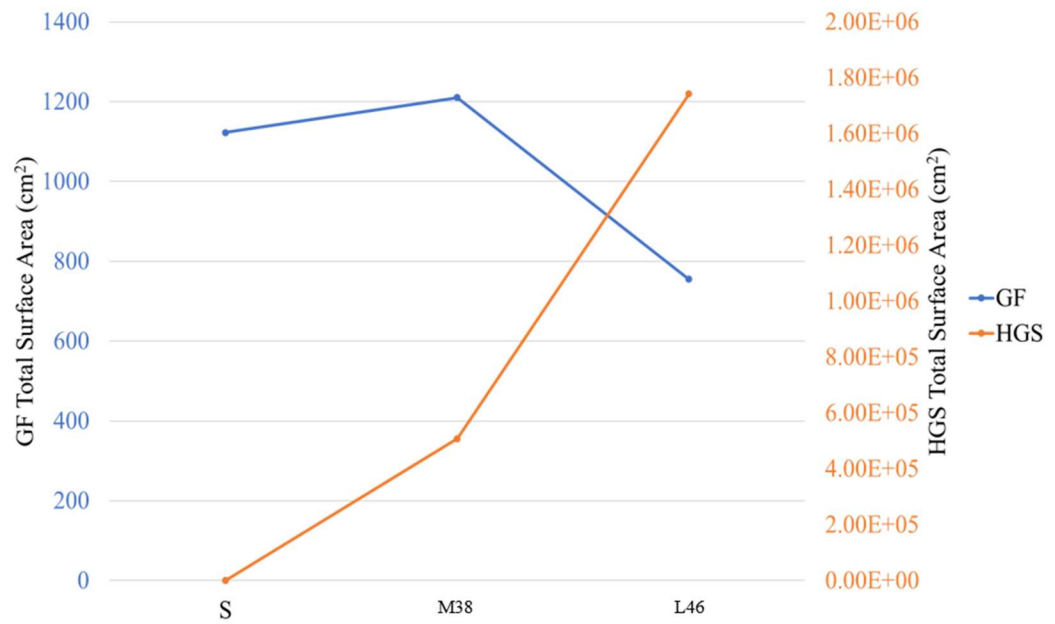


Figure 38: GF Total surface area of GF and HGS for S, M38, and L46 formulations.

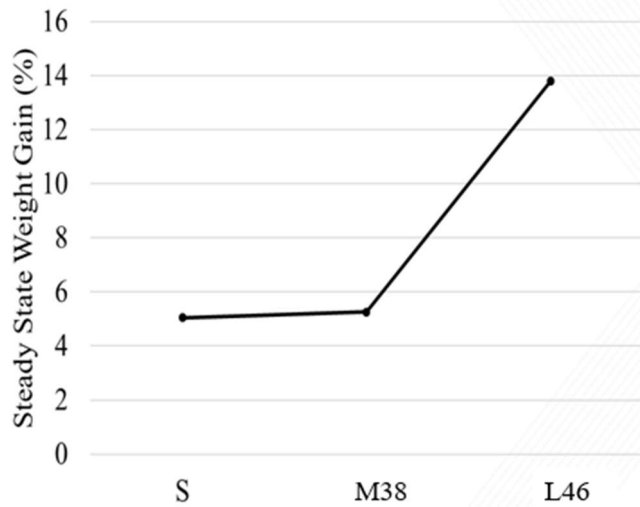


Figure 39: Steady state weight gain (%) from water uptake.

8.1.2 Effect of CaCO₃ on Water Uptake

Figure 40 shows that the CaCO₃ content lowers as composite density decreases. This is obviously due to the substitution of CaCO₃ with HGS. From Figure 39, it is evident that the absorption weight gain increases as CaCO₃ loading decreases. This could be attributed to the hydrophilicity of calcium carbonate. The wettability of calcium carbonate and glass was compared using Young's Equation in Eq. (4). In this equation, γ^{sv} is the solid/liquid interfacial free energy, γ^{sl} is the solid free energy, γ^{lv} is the liquid free energy, and θ is the contact angle. When the contact angle is low, it corresponds to a high solid/liquid interfacial free energy and, thus, good wettability. CaCO₃ has higher interfacial free energy than glass, meaning that it has greater hydrophilicity (Table 24). As a result, it may be expected that the larger amount of calcium carbonate in higher density composites may lead to a quicker saturation of the composite, causing water uptake to reach steady-state more rapidly. This is most apparent in Figure 37, where S and M38 at 800 s^(1/2) while L46 reaches steady-state at approximately 1600 s^(1/2).

$$\gamma^{sv} = \gamma^{sl} + \gamma^{lv} \cos\theta \quad \text{Eq (4)}$$

Table 24: Values of solid surface free energy, liquid surface free energy, and contact angle used to calculate solid/liquid interfacial free energy and determine wettability [55–59].

	Solid Surface Free Energy (mJ/m²) γ^{sl}	Liquid Surface Free Energy (mJ/m²) γ^{lv}	Contact Angle θ	Calculated Solid/Liquid Interfacial Free Energy (mJ/m²) γ^{sv}
CaCO ₃	57	72.2	13	122.5
Glass	65	72.2	27	43.5

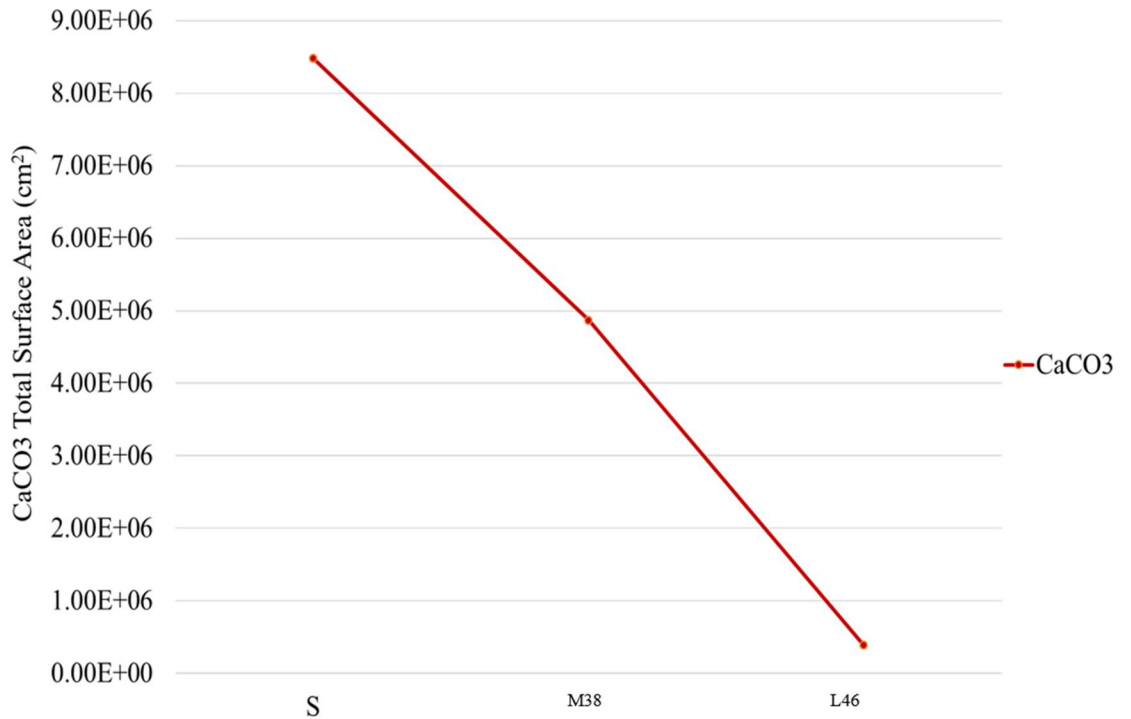


Figure 40: Total calcium carbonate (CaCO₃) surface area for S, Mδ, and Lα formulations.

Another mechanism that could contribute to this outcome is a steric effect caused by the size differentials of the additives. HGS diameters range from 25 to 44 microns while Hubercarb W4 has a median particle size of 5.9 microns. Without CaCO₃ particles to fill in between HGS, there could be more spaces for into which water could be absorbed. These mechanisms are in the process of being proven with preliminary results collected by another lab member, Edward DiLoreto. Water uptake of pure UPR and UPR with only CaCO₃ in 70°C were taken periodically for up to 22 days. UPR and UPR/CaCO₃ had 13.34% and 5.19%, respectively. Other experiments must be completed as well to understand the water uptake of each individual additive as well as the interactions between

the additives. These include water absorption of: UPR/HGS, UPR/HGS/CaCO₃, and UPR/GF.

When looking at Figure 39 and 40, it is important to note that water absorption increased to a greater extent when calcium carbonate content was closest to zero. Even when CaCO₃ content was approximately halved (from S to M38), water uptake content did not double. In fact, it stayed close to constant. However, when the CaCO₃ content got close to zero, as it did with L46, water absorption steady-state almost tripled from 5.26% to 13.8%. This could be interpreted as meaning that a lack of any considerable calcium carbonate content will substantially increase water uptake. Since CaCO₃ is hydrophilic, one would think that its presence would increase moisture absorption. However, the opposite appears to be true; that calcium carbonate will reach a maximum water uptake more quickly, causing the composite to reach steady-state at a lower water weight gain percent.

8.2 Chapter Summary

The water absorption behavior of three different composites formulations was studied in this chapter. It was found that water uptake increases as glass surface area increases and calcium carbonate surface area decreases. In other words, the low-density composite, L46, absorbed the most water compared to S and M38. This could be due to the higher glass surface area creating more interfaces or a calcium carbonate steric effect, both of which result in more areas where water can be stored. Alternatively, higher calcium carbonate content in the standard and mid-density composites, could lead to a quicker saturation, and thus an overall lower weight gain.

CHAPTER 9. CONCLUSIONS AND FUTURE WORK

9.1 Conclusions

The effects of HGS properties, loading, and surface functionalization on the mechanical properties and density of SMC GF/polyester composites were investigated. When compared to standard density composites, the medium density composites containing the M38 HGS maintained the mechanical properties to the greatest degree. Specifically, the tensile strength and tensile modulus were only 9% lower, and the flexural strength and modulus were 9% greater and 11% lower respectively compared to the corresponding properties of the standard density composites. With only a 12% and a 24% reduction in tensile strength and modulus, respectively, L46 was a formulation that produced low-density composites without greatly compromising the tensile properties. Based on the full-factorial analysis of the six formulations of interest, it was shown that the replacement of the toughening CaCO_3 with any type of HGS and any loading has no significant effect on the impact energy. However, beyond this, it could only be said that U28 has significantly lower flexural strength and modulus than L28. As a result, cost analysis was used as the basis for determining the superior formulation within this set of SMC composite experiments. The outcome of this comparison was that S is the least expensive formulation to produce, but L28 was the most cost-effective in the DOE with no significant decrease in properties.

Lastly, water absorption of fiber reinforced syntactic foams was studied. It was found that the low-density composite gained more DIW than the mid- or standard density composites. Additionally, the water uptake of the SMC composites increase is greater from

M38 to L46 than from S to M38. This may be due to the decrease in CaCO_3 which results in a steric effect or the composite absorbing more DIW before reaching saturation. As CaCO_3 decreases, HGS content increases. Higher HGS content may also increase the number interfaces into which DIW can penetrate.

9.2 Future Work

Expanding upon this research is of importance to create a resin paste system that meets industry needs, including ease of manufacturability and lightweight composites with comparable mechanical properties. The first step in understanding the effect of lightweight additives on SMC composites is to complete a correct fractional-factorial DOE. This would allow for proper statistical analysis to understand what factors and levels have a significant influence on the composite properties.

The ability to produce ultra-low density samples may be improved by using a custom designed mixing blade or by fine-tuning the viscosity. The latter could be done with the use of viscosity modifiers if this additive does not alter the final composite properties. Alternatively, deliberately selecting HGS with specific surface functionalizations that can interact with the desired matrix, as only a methacrylsilane surface chemistry was used in this study, could alter the viscosity of the resin paste or the mechanical characteristics.

To improve the mechanical properties of formulations with high HGS content while retaining their low- and ultra-low densities, one may investigate the coating of HGS in cellulose nanocrystals. This may increase the composite tensile modulus, as stiffer materials are added to the formulation, and improve the interfacial bonding between the

matrix and HGS. Lastly, functionally graded SMC composites, in which standard density plies surround low-density or ultra-low density plies, should be investigated. These have the potential to decrease water uptake of lightweight composites by creating a barrier from the higher glass surface area of the interior syntactic foam plies.

APPENDIX A. CONTOUR PLOTS

Contour plots cannot be made with discrete variables like surface functionalization. As a result, only one contour plot was produced for flexural modulus (GPa), which plotted CaCO₃ Content (vol%) vs. HGS Loading (vol%).

A.1 Flexural Modulus Contour Plot

Figure 37 illustrates a contour plot showing how CaCO₃ and HGS loading affect the flexural modulus. It is seen that, within the constraints of the limited DOE analyzed, the flexural modulus is lowest at high HGS content with a calcium carbonate volume fraction of zero. This corresponds to ultra-low density formulations.

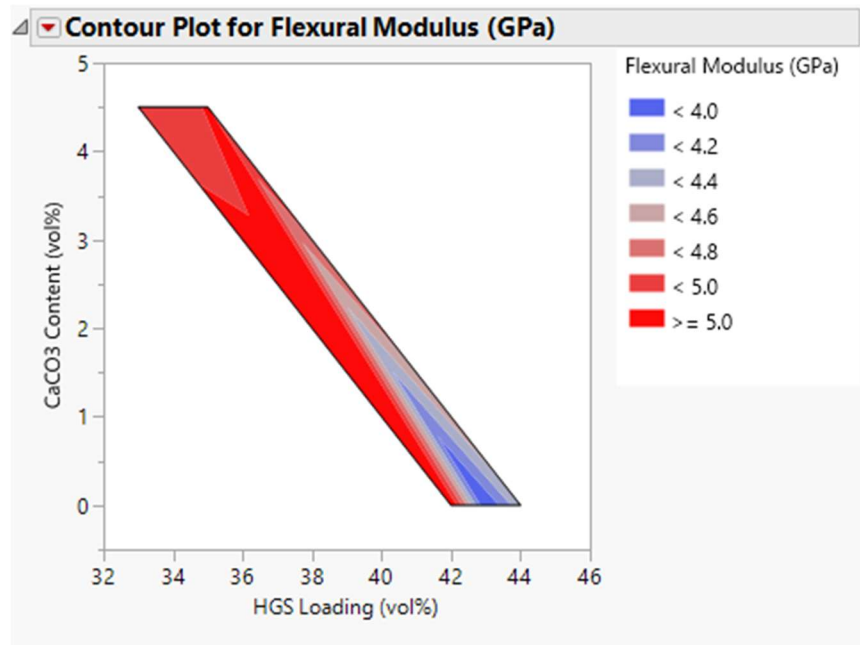


Figure 41: JMP contour plot illustrating the effect of calcium carbonate content and HGS loading on the flexural modulus.

REFERENCES

- [1] Dumont LO and PJJ. Sheet Molding Compounds (SMC) 2015:2683–718.
- [2] Asadi A, Miller M, Sultana S, Moon RJ, Kalaitzidou K. Introducing cellulose nanocrystals in sheet molding compounds (SMC). *Compos Part A Appl Sci Manuf* 2016;88:206–15. doi:10.1016/j.compositesa.2016.05.033.
- [3] Gupta N, Pinisetty D, Shunmugasamy VC. Reinforced Polymer Matrix Syntactic Foams: Effect of Nano and Micro-Scale Reinforcement. n.d.
- [4] Yalcin B. Hollow Glass Microspheres in Sheet Molding Compounds. Elsevier; 2015. doi:10.1016/B978-1-4557-7443-2.00005-0.
- [5] Pinisetty D, Shunmugasamy VC, Gupta N. Hollow Glass Microspheres in Thermosets-Epoxy Syntactic Foams. Elsevier; 2015. doi:10.1016/B978-1-4557-7443-2.00006-2.
- [6] Luong DD, Strbik OM, Hammond VH, Gupta N, Cho K. Development of high performance lightweight aluminum alloy/SiC hollow sphere syntactic foams and compressive characterization at quasi-static and high strain rates. *J Alloys Compd* 2013;550:412–22. doi:10.1016/j.jallcom.2012.10.171.
- [7] Wegner, L D LJG. Microstructural Design of Cellular Materials-II: Microsandwich Foams 1995;43:1651–67.
- [8] Ferreira JAM, Capela C, Costa JD. A study of the mechanical behaviour on fibre

- reinforced hollow microspheres hybrid composites. *Compos Part A Appl Sci Manuf* 2010;41:345–52. doi:10.1016/j.compositesa.2009.10.018.
- [9] Wouterson EM, Boey FYC, Hu X, Wong SC. Effect of fiber reinforcement on the tensile, fracture and thermal properties of syntactic foam. *Polymer (Guildf)* 2007;48:3183–91. doi:10.1016/j.polymer.2007.03.069.
- [10] Gupta N, Ye R, Porfiri M. Comparison of tensile and compressive characteristics of vinyl ester/glass microballoon syntactic foams. *Compos Part B Eng* 2010;41:236–45. doi:10.1016/j.compositesb.2009.07.004.
- [11] Oldenbo M, Fernberg SP, Berglund LA. Mechanical behaviour of SMC composites with toughening and low density additives. *Compos Part A Appl Sci Manuf* 2003;34:875–85. doi:10.1016/S1359-835X(03)00155-6.
- [12] Karthikeyan CS, Sankaran S, Kishore. Flexural behaviour of fibre-reinforced syntactic foams. *Macromol Mater Eng* 2005;290:60–5. doi:10.1002/mame.200400177.
- [13] Wang L, Zhang J, Yang X, Zhang C, Gong W, Yu J. Flexural properties of epoxy syntactic foams reinforced by fiberglass mesh and/or short glass fiber. *Mater Des* 2014;55:929–36. doi:10.1016/j.matdes.2013.10.065.
- [14] Karthikeyan CS, Sankaran S, Kishore. Elastic behaviour of plain and fibre-reinforced syntactic foams under compression. *Mater Lett* 2004;58:995–9. doi:10.1016/j.matlet.2003.08.012.

- [15] Ferreira JAM, Salviano K, Costa JD, Capela C. Fatigue behaviour in hybrid hollow microspheres/fibre reinforced composites. *J Mater Sci* 2010;45:3547–53. doi:10.1007/s10853-010-4397-4.
- [16] Karthikeyan CS, Sankaran S, Kumar MNJ. Processing and Compressive Strengths of Syntactic Foams. *Polymer (Guildf)* 2001:405–11.
- [17] Wouterson EM, Boey FYC, Hu X, Wong SC. Effect of fiber reinforcement on the tensile, fracture and thermal properties of syntactic foam. *Polymer (Guildf)* 2007;48:3183–91. doi:10.1016/j.polymer.2007.03.069.
- [18] Sauvant-Moynot V, Gimenez N, Sautereau H. Hydrolytic ageing of syntactic foams for thermal insulation in deep water: Degradation mechanisms and water uptake model. *J Mater Sci* 2006;41:4047–54. doi:10.1007/s10853-006-7618-0.
- [19] Janas VF, McCullough RL. Moisture absorption in unfilled and glass-filled, cross-linked polyester. *Compos Sci Technol* 1987;29:293–315. doi:10.1016/0266-3538(87)90077-7.
- [20] Faguaga E, Pérez CJ, Villarreal N, Rodriguez ES, Alvarez V. Effect of water absorption on the dynamic mechanical properties of composites used for windmill blades. *Mater Des* 2012;36:609–16. doi:10.1016/j.matdes.2011.11.059.
- [21] Panthapulakkal S, Sain M. Studies on the water absorption properties of short hemp-glass fiber hybrid polypropylene composites. *J Compos Mater* 2007;41:1871–83. doi:10.1177/0021998307069900.

- [22] Boinard E, Pethrick RA, Dalzel-Job J, Macfarlane CJ. Influence of resin chemistry on water uptake and environmental ageing in glass fibre reinforced composites-polyester and vinyl ester laminates. *J Mater Sci* 2000;35:1931–7. doi:10.1023/A:1004766418966.
- [23] Gu H. Dynamic mechanical analysis of the seawater treated glass/polyester composites. *Mater Des* 2009;30:2774–7. doi:10.1016/j.matdes.2008.09.029.
- [24] Camino G, Polishchuk AY, Luda MP, Revellino M, Blancon R, Martinez-Vega JJ. Water ageing of SMC composite materials: A tool for material characterisation. *Polym Degrad Stab* 1998;61:53–63. doi:10.1016/S0141-3910(97)00129-8.
- [25] Loos AC, Springer GS, Sanders BA, Tung RW. Moisture Absorption of Polyester-E Glass Composites. *J Compos Mater* 1980;14:142–54. doi:10.1177/002199838001400206.
- [26] Emissions GG, Economy F. The EPA Automotive Trends Report 2020.
- [27] Morehouse Cowles. Modern Dispersion Technology A Primer in Dispersers 2012.
- [28] Shivakumar KN, Swaminathan G, Sharpe M. Carbon/vinyl ester composites for enhanced performance in marine applications. *J Reinf Plast Compos* 2006;25:1101–16. doi:10.1177/0731684406065194.
- [29] Tekalur SA, Shivakumar K, Shukla A. Mechanical behavior and damage evolution in E-glass vinyl ester and carbon composites subjected to static and blast loads. *Compos Part B Eng* 2008;39:57–65. doi:10.1016/j.compositesb.2007.02.020.

- [30] Feraboli P, Peitso E, Deleo F, Cleveland T, Stickler PB. Characterization of prepreg-based discontinuous carbon fiber/epoxy systems. *J Reinf Plast Compos* 2009;28:1191–214. doi:10.1177/0731684408088883.
- [31] Kessler M, Roggendorf C, Schnettler A. Investigation of the physical properties of elastic syntactic foams. *Conf Rec IEEE Int Symp Electr Insul* 2012:526–30. doi:10.1109/ELINSL.2012.6251525.
- [32] Roques-Carmes T, Marchal P, Gigante A, Corbel S. Stereolithography fabrication and characterization of syntactic foams containing hollow glass microspheres. *Russ Chem Rev* 2009;78:375–86. doi:10.1070/rc2009v078n04abeh003897.
- [33] IDI Composites International. IDI Composites 2013.
- [34] Mishra S, Mohanty AK, Drzal LT, Misra M, Parija S, Nayak SK, et al. Studies on mechanical performance of biofibre/glass reinforced polyester hybrid composites. *Compos Sci Technol* 2003;63:1377–85. doi:10.1016/S0266-3538(03)00084-8.
- [35] Pang Y, Curtis TE, Luo S, Huang D. Exfoliated Graphene Leads to Exceptional 2019. doi:10.1021/acsnano.8b04734.
- [36] Asadi A, Baaj F, Mainka H, Rademacher M, Thompson J, Kalaitzidou K. Basalt fibers as a sustainable and cost-effective alternative to glass fibers in sheet molding compound (SMC). *Compos Part B Eng* 2017;123:210–8. doi:10.1016/j.compositesb.2017.05.017.
- [37] IDI Composites International. S80 Series SMC Datasheet 2016.

- [38] Devi LU, Bhagawan SS, Thomas S. Mechanical properties of pineapple leaf fiber-reinforced polyester composites. *J Appl Polym Sci* 1997;64:1739–48. doi:10.1002/(sici)1097-4628(19970531)64:9<1739::aid-app10>3.3.co;2-o.
- [39] Asadi A, Miller M, Singh A V., Moon RJ, Kalaitzidou K. Lightweight sheet molding compound (SMC) composites containing cellulose nanocrystals. *Compos Struct* 2017;160:211–9. doi:10.1016/j.compstruct.2016.10.051.
- [40] Wouterson EM, Boey FYC, Hu X, Wong SC. Specific properties and fracture toughness of syntactic foam: Effect of foam microstructures. *Compos Sci Technol* 2005;65:1840–50. doi:10.1016/j.compscitech.2005.03.012.
- [41] Gupta N, Nagorny R. Tensile properties of glass microballoon-epoxy resin syntactic foams. *J Appl Polym Sci* 2006;102:1254–61. doi:10.1002/app.23548.
- [42] He S, Carolan D, Fergusson A, Taylor AC. Toughening epoxy syntactic foams with milled carbon fibres: Mechanical properties and toughening mechanisms. *Mater Des* 2019. doi:10.1016/j.matdes.2019.107654.
- [43] Huang, J. S., Gibson LJ. Elastic Moduli of a Composite of Hollow Spheres in a Matrix. *Current* 1993;41. doi:10.1016/0022-5096(93)90063-L.
- [44] Hu G, Yu D. Tensile, thermal and dynamic mechanical properties of hollow polymer particle-filled epoxy syntactic foam. *Mater Sci Eng A* 2011;528:5177–83. doi:10.1016/j.msea.2011.03.071.
- [45] Liang JZ, Li RKY. Mechanical properties and morphology of glass bead-filled

- polypropylene composites. *Polym Compos* 1998;19:698–703.
doi:10.1002/pc.10142.
- [46] Tagliavia G, Porfiri M, Gupta N. Analysis of flexural properties of hollow-particle filled composites. *Compos Part B Eng* 2010;41:86–93.
doi:10.1016/j.compositesb.2009.03.004.
- [47] Mutua FN, Lin P, Koech JK, Wang Y. Surface Modification of Hollow Glass Microspheres. *Mater Sci Appl* 2012;03:856–60. doi:10.4236/msa.2012.312125.
- [48] Zhang L, Ma J. Effect of coupling agent on mechanical properties of hollow carbon microsphere/phenolic resin syntactic foam. *Compos Sci Technol* 2010;70:1265–71.
doi:10.1016/j.compscitech.2010.03.016.
- [49] Ferreira JAM, Capela C, Costa JD. A study of the mechanical behaviour on fibre reinforced hollow microspheres hybrid composites. *Compos Part A Appl Sci Manuf* 2010;41:345–52. doi:10.1016/j.compositesa.2009.10.018.
- [50] Wouterson EM, Boey FYC, Hu X, Wong SC. Fracture and impact toughness of syntactic foam. *J Cell Plast* 2004;40:145–54. doi:10.1177/0021955X04041960.
- [51] Kim HS, Mitchell C. Impact performance of laminates made of syntactic foam and glass fiber reinforced epoxy as protective materials. *J Appl Polym Sci* 2003;89:2306–10. doi:10.1002/app.12470.
- [52] Guo Y, Simpson JR, Pignatiello JJ. Construction of efficient mixed-level fractional factorial designs. *J Qual Technol* 2007;39:241–57.

doi:10.1080/00224065.2007.11917691.

- [53] Dhakal HN, Zhang ZY, Richardson MOW. Effect of water absorption on the mechanical properties of hemp fibre reinforced unsaturated polyester composites. *Compos Sci Technol* 2007;67:1674–83. doi:10.1016/j.compscitech.2006.06.019.
- [54] Science P, Suwon J, Changwon M. Equilibrium Water Uptake of Epoxy / Carbon Fiber Composites in Hygrothermal Environmental Conditions 2000;35:264–78. doi:10.1106/BMD1-N6PA-4JDD-C6G9.
- [55] Calhoun A, College W, Walla W, Chiang E. Determination of the Surface Energetics of Surface Modified Calcium Carbonate Using Inverse Gas Chromatography 2006. doi:10.1002/vnl.
- [56] Kini R, Larsen R. Petroleum hydrate deposition mechanisms : The influence of pipeline wettability PETROLEUM HYDRATE DEPOSITION MECHANISMS : THE INFLUENCE OF PIPELINE WETTABILITY 2015.
- [57] Knowledge T. TYPICAL VALUES OF SURFACE ENERGY FOR MATERIALS AND 2020:1–5.
- [58] Wang C, Piao C, Zhai X, Hickman FN, Li J. Synthesis and Characterization of Hydrophobic Calcium Carbonate Particles via a Dodecanoic Acid Inducing Process Synthesis and characterization of hydrophobic calcium carbonate particles via a dodecanoic acid inducing process. *Powder Technol* 2010;198:131–4. doi:10.1016/j.powtec.2009.10.026.

- [59] Tan KT, White CC, Hunston DL, Clerici C, Steffens KL, Goldman J, et al. Fundamentals of Adhesion Failure for a Model Adhesive (PMMA / Glass) Joint in Humid Environments 2008;8464. doi:10.1080/00218460802004428.